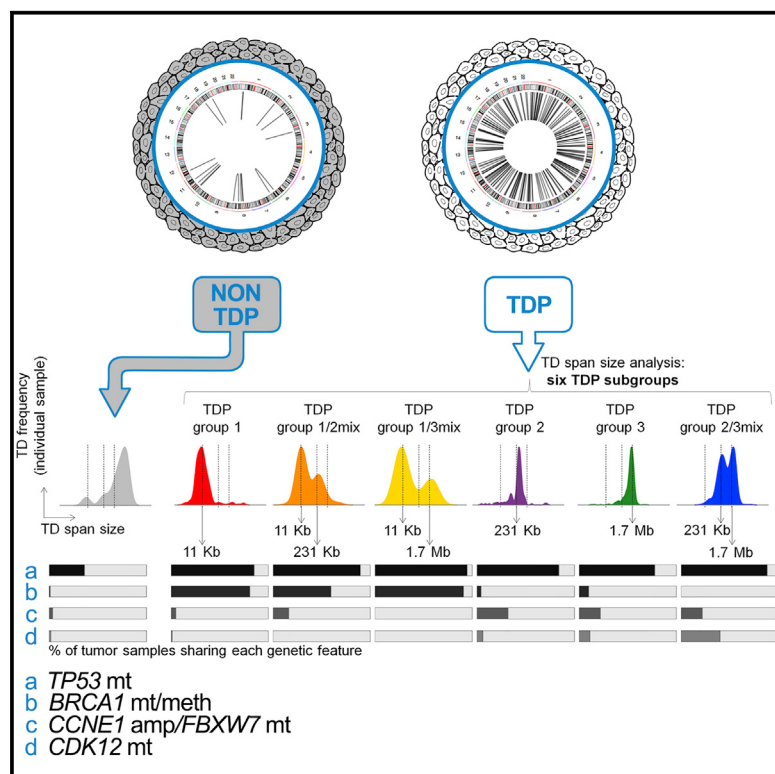


Cancer Cell

The Tandem Duplicator Phenotype Is a Prevalent Genome-Wide Cancer Configuration Driven by Distinct Gene Mutations

Graphical Abstract



Authors

Francesca Menghi, Floris P. Barthel,
Vinod Yadav, ..., Roel G.W. Verhaak,
Jos Jonkers, Edison T. Liu

Correspondence

ed.liu@jax.org

In Brief

Menghi et al. stratify tandem duplicator phenotype tumors by classifying their tandem duplications (TDs) into three span sizes associated with different pathway alterations and show how TDs disrupt tumor suppressors and chromatin topologically associating domains while duplicating oncogenes and super-enhancers.

Highlights

- Abundant and distributed tandem duplications form a distinct chromotype in cancer
- Six recurrent tandem duplicator phenotypes (TDPs) are characterized by TD span size
- Conjoint abrogation of *BRCA1* and *TP53* causes TDPs with ~11 kb TDs
- CCNE1* pathway activation and *CDK12* mutations associate with ~231 kb and ~1.7 Mb TDs



The Tandem Duplicator Phenotype Is a Prevalent Genome-Wide Cancer Configuration Driven by Distinct Gene Mutations

Francesca Menghi,¹ Floris P. Barthel,¹ Vinod Yadav,¹ Ming Tang,² Bo Ji,³ Zhonghui Tang,¹ Gregory W. Carter,³ Yijun Ruan,¹ Ralph Scully,⁴ Roel G.W. Verhaak,¹ Jos Jonkers,⁵ and Edison T. Liu^{3,6,*}

¹The Jackson Laboratory for Genomic Medicine, Farmington, CT 06030, USA

²MD Anderson Cancer Center, Houston, TX 77030, USA

³The Jackson Laboratory, Bar Harbor, ME 04609, USA

⁴Division of Hematology Oncology, Department of Medicine, and Cancer Research Institute, Beth Israel Deaconess Medical Center and Harvard Medical School, Boston, MA 02215, USA

⁵Oncode Institute and Division of Molecular Pathology, The Netherlands Cancer Institute, Amsterdam 1066CX, the Netherlands

⁶Lead Contact

*Correspondence: ed.liu@jax.org

<https://doi.org/10.1016/j.ccel.2018.06.008>

SUMMARY

The tandem duplicator phenotype (TDP) is a genome-wide instability configuration primarily observed in breast, ovarian, and endometrial carcinomas. Here, we stratify TDP tumors by classifying their tandem duplications (TDs) into three span intervals, with modal values of 11 kb, 231 kb, and 1.7 Mb, respectively. TDPs with ~11 kb TDs feature loss of *TP53* and *BRCA1*. TDPs with ~231 kb and ~1.7 Mb TDs associate with *CCNE1* pathway activation and *CDK12* disruptions, respectively. We demonstrate that p53 and BRCA1 conjoint abrogation drives TDP induction by generating short-span TDP mammary tumors in genetically modified mice lacking them. Lastly, we show how TDs in TDP tumors disrupt heterogeneous combinations of tumor suppressors and chromatin topologically associating domains while duplicating oncogenes and super-enhancers.

INTRODUCTION

Whole-genome sequencing (WGS) of large numbers of human cancers has revealed recurrent patterns of highly complex genomic rearrangements, such as chromothripsis and chromoplexy (Baca et al., 2013; Stephens et al., 2011). Recently, three groups have described an enrichment of head-to-tail somatic segmental tandem duplications (TDs) primarily associated with breast and ovarian cancers, which is commonly referred to as the tandem duplicator phenotype (TDP) (Glodzik et al., 2017; Menghi et al., 2016; Menghi and Liu, 2016; Nik-Zainal et al., 2016; Popova et al., 2016). These early reports have shown a sta-

tistical association between the TDP and loss of *BRCA1* in breast cancers (Menghi and Liu, 2016; Nik-Zainal et al., 2016), loss of *TP53* and overexpression of certain cell cycle and DNA replication genes primarily in breast and ovarian cancers (Menghi et al., 2016), and mutations of the *CDK12* gene in a small subgroup of ovarian cancers (Popova et al., 2016). These analyses also noted that, within the TDP cancer genomes, TD span sizes are clustered around specific lengths, which can be used to classify distinct genomic subtypes of TDP. In fact, we have shown that TDP tumors can be separated into at least two major subgroups: TDP group 1 tumors are *BRCA1*-deficient and feature short-span TDs (~10 kb), whereas TDP group 2 tumors are *BRCA1*

Significance

Whole-genome sequencing has revealed recurrent patterns of DNA rearrangements occurring on a genome-wide scale. Here we provide a detailed analysis of one such pattern, the tandem duplicator phenotype (TDP), characterized by an enrichment of genetically distributed head-to-tail somatic segmental tandem duplications. Through a meta-analysis of over 2,700 human cancer genomes, we develop a classification algorithm that distinguishes six forms of TDP, each one associated with specific genetic abnormalities and consequential genomic rearrangements. We show that conjoint abrogation of *BRCA1* and *TP53* drives the emergence of a precise TDP state with short-span duplications and frequently results in tumor suppressor gene disruption. Conversely, activation of the *CCNE1* pathway and *CDK12* mutations result in the duplication of oncogenes and tissue-specific regulatory elements.



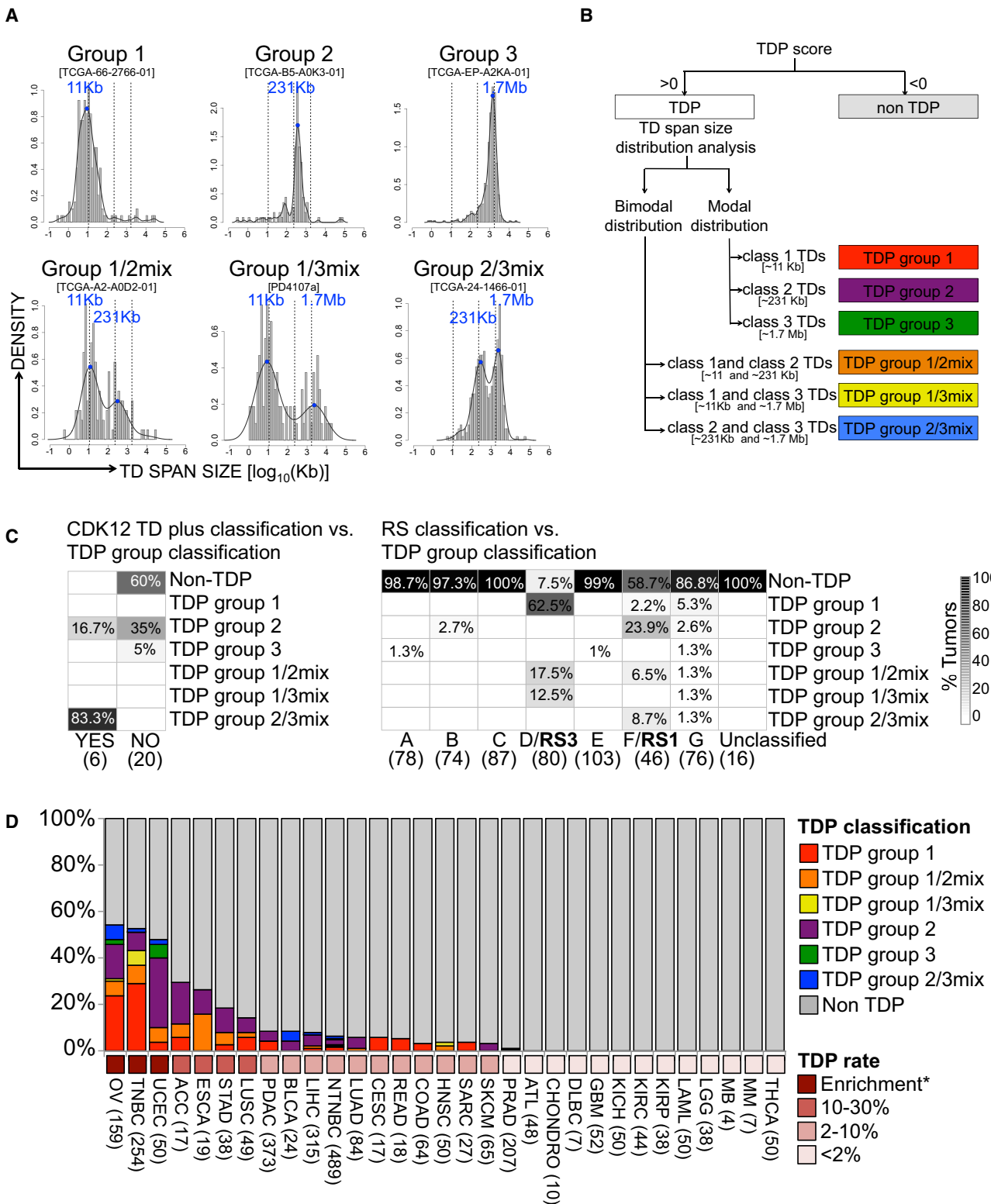


Figure 1. Classification of TDP Genomes into Six Distinct Subgroups

Figure 1. Classification of TDP Genomes into Six Distinct Subgroups
 (A) Representative TD span size distribution profiles for the six identified TDP subgroups. Individual distribution peaks are highlighted in blue. Vertical lines indicate the three modal span sizes at 11 kb, 231 kb, and 1.7 Mb.

(B) Schematic overview of the TDP group classification approach.

(legend continued on next page)

wild-type and feature medium-span TDs (\sim 50–600 kb) (Menghi et al., 2016; Menghi and Liu, 2016). Similarly, Nik-Zainal et al. (2016), examining over 500 breast cancer samples, described two TD-based rearrangement signatures (RS), RS1 and RS3, characterized by TDs of distinct sizes: >100 kb (RS1) and <10 kb (RS3) with RS3 but not RS1 strongly correlating with loss of BRCA1. Popova et al. (2016) reported the “TD plus” phenotype in some ovarian cancers featuring a large number of somatic TDs with span distribution modes at 300 kb and 3 Mb associated with disruptive CDK12 mutations.

Here, we propose to unify all of these separate observations through a meta-analysis of cancer genomes representing a variety of tumor types, aiming to identify the genetic drivers that converge on creating the TDP and to define the structural impact of TDs on the cancer genome.

RESULTS

TD Span Distribution Profiles Classify TDP Tumors into Six Distinct Subgroups

To explore the different configurations of the TDP in detail, we first analyzed TD number and genomic distribution (i.e., TDP score [Menghi et al., 2016]) across the entire Cancer Genome Atlas (TCGA) WGS dataset, comprising 25 distinct tumor types. Of the 992 TCGA cancer genomes analyzed, 118 (11.9%) were classified as TDP (Table S1). We examined the TD span size distribution of each individual TDP tumor and observed only a few recurrent patterns, each one characterized by either a modal or a bimodal profile (Figure 1A). We systematically classified these recurrent profiles by binning all of the modal peaks relative to the TD span size distributions observed across 118 identified TDP tumors in this dataset into five non-overlapping intervals, based on the best fit of a Gaussian finite mixture model (see the STAR Methods). We then labeled the TDs corresponding to the five span size intervals as class 0: <1.6 kb in span size; class 1: between 1.64 and 51 kb (median value of 11 kb); class 2: between 51 and 622 kb (median value of 231 kb); class 3: between 622 kb and 6.2 Mb (median value of 1.7 Mb); and class 4: >6.2 Mb (Figure S1). Noticeably, classes 1–3 made up almost 95% (146/154) of all the identified modal peaks (Table S2).

Using this classification, we were able to stratify TDP tumors into six distinct subgroups. Tumors with a modal TD span size distribution were designated as TDP group 1, group 2, or group 3, based on the presence of a single class 1 (11 kb), class 2 (231 kb), or class 3 (1.7 Mb) TD span size distribution peak, respectively. Tumors that showed a bimodal TD span size profile were designated as TDP group 1/2mix (featuring both a class 1 and a class 2 TD span size distribution peaks), group 1/3mix (class 1 and class 3 peaks), or group 2/3mix (class 2 and class 3 peaks; Figures 1A and 1B). Only 1/118 tumors (0.8%) could not be classified into any of the six identified TDP subgroups, since it featured only very small or very large TDs (<1.6 kb, i.e., class 0; and >6.2 Mb, i.e., class 4), and was excluded from

further analysis. Thus, virtually all of the TDP tumors analyzed exhibited clearly distinct TD span size distributions converging on one of only three highly recurrent and narrowly ranged span size intervals. These data strongly suggest that specific, distinct mechanisms of DNA instability are at play in the identified TDP subgroups.

When compared with the recently described TD-based genomic signatures (Nik-Zainal et al., 2016; Popova et al., 2016), our TDP classification algorithm classified 83% (5/6) of the reported CDK12 TD plus phenotype-positive tumors as TDP group 2/3mix (Figure 1C). It also classified 93% (74/80) of RS3-positive tumors as TDP groups 1, 1/2mix, or 1/3mix; but only 39% (18/46) of RS1-positive tumors as TDP group 2, 1/2mix, or 2/3mix, with most of the remaining 61% (27/46) classifying as non-TDP (Figure 1C). On closer inspection, most of the tumors classified as RS1 that were not designated as TDP featured only a small number of TDs (<15), and did not pass the TDP score threshold. Since our threshold was defined by a statistical segregation of a distinctive cancer genomic configuration, these subthreshold RS1-positive tumors are likely not to represent a specific mechanistic origin but a general characteristic of cancer. Thus, collectively, there is a consensus that a specific form of genomic instability characterized by accumulation of TDs, which we call the TDP, exists in cancer. Our classification approach, however, simplifies and unifies the identification of the TDP by generating a single score and provides refined subclassifications based on TD span size.

TDP Subgroups Occur at Different Frequencies across Different Tumor Types

We validated our classification scheme on a separate pan-cancer dataset of whole-genome sequences relative to 1,725 tumor samples from individual patient donors, assembled from 30 independent studies (see the STAR Methods and Table S3). A total of 258/1725 (15%) tumors were classified as TDP, and over 99% of these (257/258) matched one of the six identified TDP subgroup profiles (Table S3), indicating that our classification scheme performs consistently and robustly across different tumor types and datasets.

When combined with the TCGA training set, we analyzed a total of 2,717 independent tumor genomes, of which 375 (13.8%) classified as TDP (Table S1). Using this large dataset, we confirmed that the TDP is not a ubiquitous characteristic of cancer. In fact, whereas the TDP occurred in ~50% of triple-negative breast cancer (TNBC), ovarian carcinoma (OV), and endometrial carcinoma (UCEC), it was found in 10%–30% of adrenocortical, esophageal, stomach, and lung squamous carcinomas, and in only 2%–10% of a variety of other cancer types including pancreatic, liver, non-triple-negative breast, and colorectal carcinomas. Finally, the TDP was absent in leukemia, lymphoma, glioblastoma, prostate, and thyroid carcinomas, and all forms of kidney cancer (Figure 1D; Table S1). Of note, the six TDP subgroups recurred among the few highly TDP-enriched

(C) Left: convergence between the TDP group 2/3mix profile and tumors classified as CDK12 TD-plus by Popova et al. (2016). Right: overlap between the TDP classification and RS3- and RS1-positive tumors as defined by Nik-Zainal et al. (2012). Numbers in parenthesis indicate the sample size for each tumor subclass. (D) Bar chart of the relative proportion of each TDP group across the 31 tumor types examined. *Binomial test statistics was applied to identify tumor types that are overall enriched or depleted for the TDP.

See also Figure S1, and Tables S1, S2, and S3.

tumor types, but at significantly different relative frequencies (Figure 1D). Whereas the TDP was found in almost half of all TNBC, OV, and UCEC tumors (52.8%, 54.1%, and 48%, respectively), TDP group 1 accounted for 29% (74/254) of all TNBCs and 24% (38/159) of OV cancers, but only for 4% (2/50) of UCEC tumors. Conversely, 30% of UCEC but only 7% of TNBCs and 15% of OV cancers classified as TDP group 2 (Figure 1D; Table S1). Intriguingly, the vast majority of TDP UCEC tumors were of serous histology (66.7% versus 11.5% of non-TDP tumors, $p = 9.6 \times 10^{-5}$; Fisher's test) and were highly enriched for the copy-number high-molecular subtype (91.6% versus 19.2% of non-TDP tumors, $p = 1.8 \times 10^{-7}$), while being depleted for the microsatellite instability (MSI) profile (4.2% versus 34.6% of non-TDP tumors, $p = 0.01$) (Cancer Genome Atlas Research Network et al., 2013). Taken together, these observations suggest that certain defined molecular differences must exist that guide the formation of the distinct TDP subtypes, which are distinct from those associated with the MSI form of genomic instability.

Joint Abrogation of Both BRCA1 and p53 Specifically Drives the Emergence of the TDP Group 1 Configuration

When we looked for specific mutations that may distinguish the different TDP profiles, the most prominent observation was that TDP subgroups characterized by a prevalence of short-span TDs (class 1, ~11 kb), either alone (i.e., TDP group 1) or in combination with larger TDs (i.e., TDP groups 1/2mix and 1/3mix), were tightly associated with BRCA1 deficiencies, including somatic (8.4%) or germline gene mutation (48.7%), promoter hyper-methylation (42%), or structural rearrangement (0.9%) (Figure 2A). Indeed, in the pan-cancer dataset, <2% of non-TDP tumors showed BRCA1 deficiencies, compared with 80.9% of TDP group 1, 60% of TDP group 1/2mix, and 90.9% of TDP group 1/3mix tumors. Importantly, this association was even stronger when analyzing the TNBC and OV datasets individually, where BRCA1 abrogation was present in at least 75% and up to 100% of tumors in TDP groups 1, 1/2mix, and 1/3mix (Figure 2A; Table S4). By contrast, less than 10% of non-TDP and TDP groups 2 or 3 tumors across the TNBC and OV datasets showed BRCA1 deficiencies.

Whereas BRCA1 deficiency highly enriched for TDP profiles comprising predominantly short-span TDs, either alone or in combination with larger TDs, BRCA2 disruptions were not statistically linked to any TDP configurations (Figure S2A). In fact, we found BRCA2 mutations to be significantly depleted from TDP group 1 in the pan-cancer dataset and from TDP groups 1 and 2 in the OV dataset (Figure S2A; Table S4), corroborating our previous finding of decreased BRCA1, but not BRCA2, expression levels in TDP tumors (Menghi et al., 2016).

When considering the entire pan-cancer dataset, we observed a second highly prevalent mutation associated with TDP: TP53 featured significantly higher rates of somatic mutations in all TDP groups versus non-TDP tumors (86.3% mutation rate in TDP versus 36.7% in non-TDP; Figure S2B) and across each distinct TDP subgroup when compared with non-TDP tumors (36.7% mutation rate in non-TDP versus 85.6% in TDP group 1, 84.1% in TDP group 2, 77.8% in TDP group 3, 90.2% in TDP group 1/2mix, 94.7% in TDP group 1/3mix, and 88.9% in TDP group 2/3mix; Figure 2B and Table S4). Of note, these significant

associations persisted after adjusting for BRCA1 status in a multivariate analysis (Table S4). Statistical association between TP53 mutational status and TDP could not be found when analyzing the TNBC and OV datasets separately only because TP53 is mutated in virtually 100% of TNBC (194/226; Table S4) and OV (138/140; Table S4). However, a strong association between functional loss of TP53 and TDP status was observed in the UCEC dataset, where >85% of TDP group 2 tumors have a somatic mutation of TP53 compared with <28% of non-TDP tumors (Figure 2B; Table S4). Taken together, these data suggest that TP53 mutations are necessary but not sufficient for the development of all forms of TDP-related genomic instabilities. Importantly, the conjoint abrogation of both p53 and BRCA1 was found in >72% of all TNBC and OV TDP samples with class 1 TDs (i.e., TDP groups 1, 1/2mix, and 1/3mix), but only in <10.5% of all other TDP groups and <4.7% in non-TDP tumors (Figure S2C; Table S4), suggesting that TDPs with class 1 TDs may require both proteins to be abrogated for TDP formation.

Using genetically modified mouse models of mammary cancer, we sought to definitely determine the roles of p53, BRCA1, and BRCA2 in generating the genomic pattern typical of TDP group 1. We analyzed the genomes of 18 mouse breast cancers caused by the targeted tissue-specific deletion of *Trp53* alone (KP, n = 3; WP, n = 3) or in combination with *Brca1* (KB1P, n = 3; WB1P, n = 3), *Brca2* (KB2P, n = 3) or both *Brca1* and *Brca2* (KB1B2P, n = 3) (Jonkers et al., 2001; Liu et al., 2007). Using the identical scoring algorithm for TDP as used in human tumor samples, we found the precise configuration of TDP group 1 only in tumors with homozygous deletions of both *Trp53* and *Brca1* (Figure 2C; Table S5). However, there was no evidence of combined modal peaks represented by the group 1/2mix and 1/3mix configurations. Of the six tumors specifically testing the combined homozygous deletion of *Trp53* and *Brca1* showing a *Trp53*^{Δ/Δ}; *Brca1*^{Δ/Δ} genotype, five were classified as TDP group 1. Similar to the human TDP group 1 tumors, the murine mammary cancers exhibited short TD spans of 2.5–11 kb (median value = 6.3 kb; Figure 2D). The remaining *Trp53*^{Δ/Δ}; *Brca1*^{Δ/Δ} tumor that was not scored as TDP had the appropriate TD class 1 modal peak but did not achieve the strict numerical threshold to be called a TDP tumor (TDP score = -0.23, with cut off being 0) (Figures 2C). None of the tumors arising from sole disruption of *Trp53*, or of *Trp53* and *Brca2*, showed any TDP characteristics (Figure 2C; Table S5). In tumors arising from mice with the intention of knocking out *Trp53*, *Brca1*, and *Brca2* simultaneously, we observed that whereas *Trp53* and *Brca2* were affected by homozygous deletions across all three tumors, *Brca1* was found to exhibit homozygous deletion in only one tumor. Importantly, this was the only tumor among the three that classified as TDP group 1. The remaining two tumors were non-TDP and maintained either one or both functional copies of *Brca1* (Figure 2C; Table S5). These data provide the experimental proof that the TDP group 1 configuration is a universal and specific feature of BRCA1-linked breast tumorigenesis, emerging in the context of a *TP53* null genotype. This also implies that *BRCA1* haplo-insufficiency is not sufficient to induce the TDP in the presence of *TP53* loss, despite recent evidence that it may indeed contribute to the transformation of normal mammary epithelial cells (Pathania et al., 2011). Also, not only does *BRCA2* deficiency not induce any form of TDP,

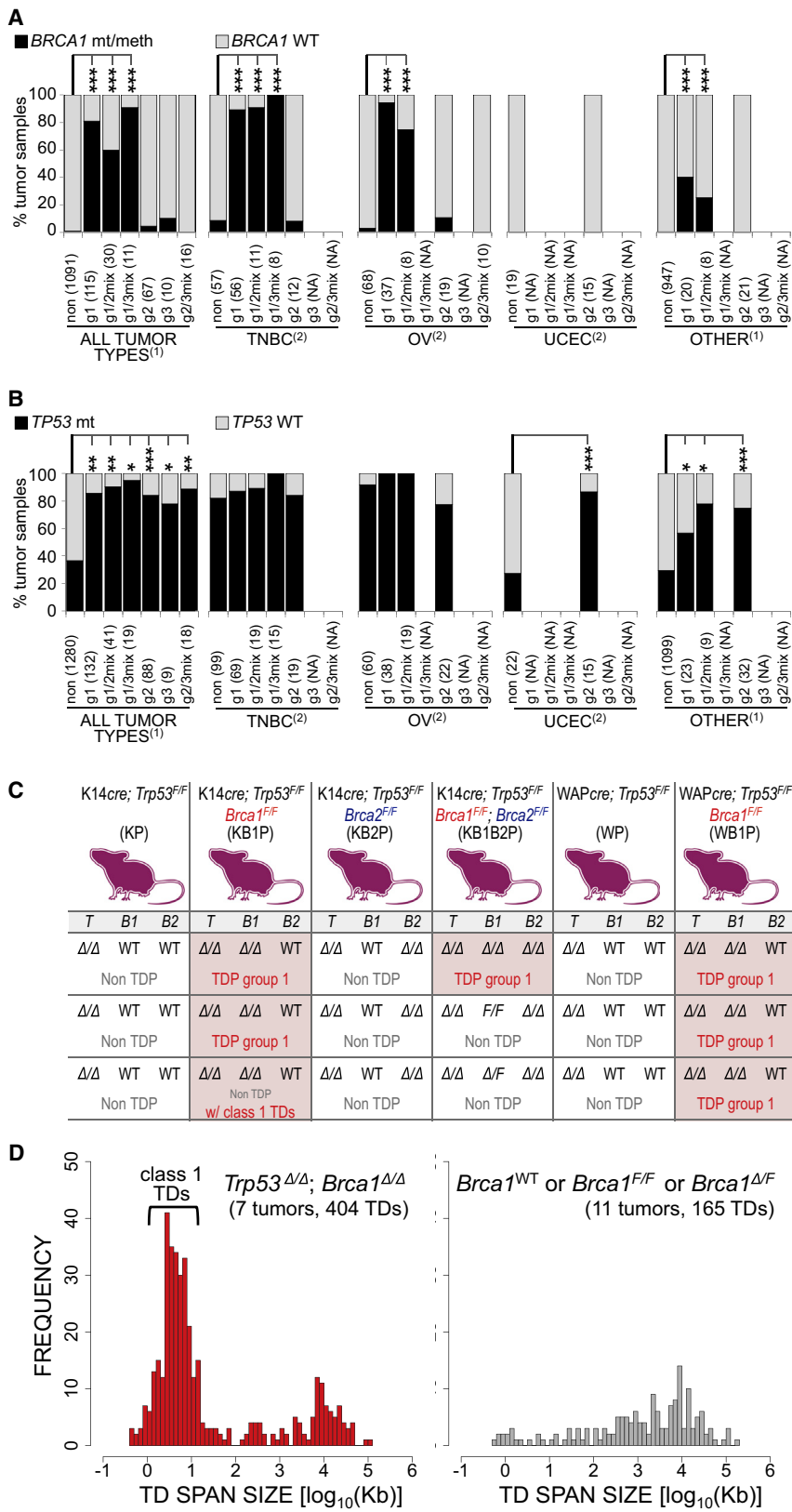


Figure 2. Conjoint Abrogation of *BRCA1* and *TP53* Results in TDP with Class 1 TDs

(A) Percentage of tumor samples with abrogation of the *BRCA1* gene. Only tumor type/TDP group combinations comprising at least eight samples were analyzed. NA, data not available; non, non-TDP; g1, g1/2mix, g1/3mix, g2, g3, g2/3mix; TDP groups 1, 1/2mix, 1/3mix, 2, 3, and 2/3mix; OTHER: all tumor types except TNBC, OV, and UCEC.

(B) Percentage of tumor samples with *TP53* somatic mutations. Annotations as in (A). Number of samples for each tumor type/TDP group combination do not necessarily match those reported in (A) because of missing values.

(C) TDP classification for mouse breast cancers with somatic loss of *Trp53* and/or *Brca1/2*. *T*, *Trp53*; *B1*, *Brca1*; *B2*, *Brca2*.

(D) Span sizes of TDs found in *Trp53/Brca1* null tumors (left) and in *Brca1*-proficient tumors (right).

***p < 0.001, **p < 0.01, *p < 0.05, by (1) generalized linear mixed model with tumor type as the random effect or (2) Fisher's exact test. See also Figure S2 and Tables S4 and S5.

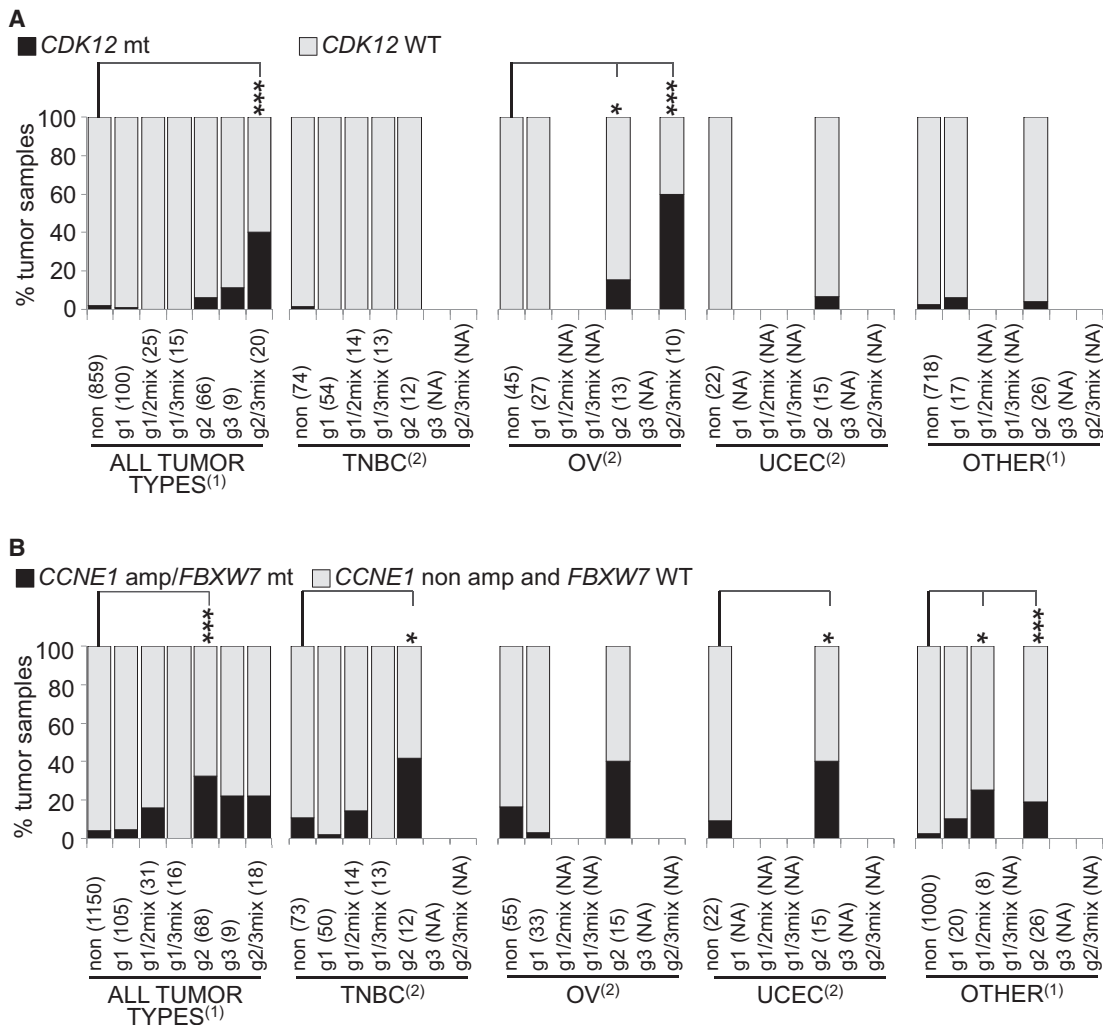


Figure 3. Genetic Perturbations Associated with BRCA1-Proficient TDP Groups

(A) Percentage of tumor samples with damaging mutations affecting *CDK12*.

(B) Percentage of tumor samples showing CCNE1 pathway activation (*FBXW7* somatic mutation or *CCNE1* amplification).

Annotations as in Figure 2A. ***p < 0.001, *p < 0.05, by (1) generalized linear mixed model with tumor type as the random effect or (2) Fisher's exact test. See also Tables S4 and S6, and Figure S3.

our observations suggest that abrogation of *BRCA2* does not suppress TD formation in the presence of *BRCA1* deficiency. Finally, the absence of any bimodal peak configurations (i.e., TDP groups 1/2mix or 1/3mix) in the mouse tumors suggests that additional mutations may be necessary to drive the mixed forms of TDP.

Identification of the Genetic Perturbations Driving Non-BRCA1-Linked TDP Groups

To identify potential genetic drivers for the non-BRCA1-linked TDPs, we compared rates of gene perturbation by somatic single nucleotide variation across different TDP subgroups. In the initial discovery phase, we analyzed tumor samples in the breast, OV, and UCEC cancer datasets, which comprised the highest number of TDP tumors, and compared individual gene mutation rates across tumor subgroups, searching for genes whose mutation rate was significantly higher in non-BRCA1-linked TDP groups

compared with TDP group 1 and with non-TDP tumors (see the [STAR Methods](#)). *CDK12* emerged as the strongest candidate linked to the TDP group 2/3mix profile, showing disruptive mutations in 26.7% of TDP group 2/3mix tumors, compared with 0% of TDP group 1 ($p = 2.3 \times 10^{-4}$, Fisher's test) and <1% of non-TDP tumors ($p = 4.0 \times 10^{-5}$, Fisher's test; [Figure S3A](#)). Also, as reported previously ([Popova et al., 2016](#)), when looking at *CDK12* mutation rates within individual tumor types, the highest frequency of mutation occurred in the OV subset, where disruption of *CDK12* by somatic mutation explained 60% (6/10) of all TDP group 2/3mix tumors, but was absent in TDP group 1 (0/27) and in non-TDP (0/45) tumors ([Figure 3A; Table S4](#)). Taken together, these results confirm the existence of a *CDK12*-linked genomic instability profile characterized by TDs of specifically large span size.

When focusing on TDP group 2 tumors, the strongest association involved *FBXW7*, which was mutated in 11.5% of TDP

group 2 tumors, compared with 2.1% of TDP group 1 ($p = 2.3 \times 10^{-2}$, Fisher's test) and 1.3% of non-TDP tumors ($p = 4.4 \times 10^{-4}$; Figure S3B). Although significant, the disruption of *FBXW7* could only explain a modest fraction of all TDP group 2 tumors. We therefore hypothesized that other genes may contribute to this profile by virtue of copy-number variation (CNV). To explore this possibility, we focused on the TCGA dataset and examined CNV profiles that might be associated with TDP group 2 using a linear mixed model analysis (see the STAR Methods). The top six genes ranked in this analysis were all part of the 19q12 amplicon that is frequently found in ovarian, breast, and endometrial carcinomas, and that comprises *CCNE1* (Etemadmoghadam et al., 2013) (Figure S3C; Table S6). The *FBXW7* protein is known to act as a negative regulator of *CCNE1* activity by binding directly to the *CCNE1* protein and targeting it for ubiquitin-mediated degradation (Klotz et al., 2009). Thus, *FBXW7* disruptive mutations might phenocopy *CCNE1* amplification, therefore independently contributing to the same oncogenic pathway. When assessing the frequency of *CCNE1* pathway activation defined by the presence of either *FBXW7* somatic damaging mutations or *CCNE1* amplification (≥ 6 gene copies), 32.4% of TDP group 2 tumors scored positively, compared with <5% of non-TDP tumors and TDP group 1 tumors (Figure 3B; Table S4). Specifically, in each one of the individual TNBC, OV, and UCEC datasets, *CCNE1* pathway activation was found to explain at least 40% of TDP group 2 tumors (Figure 3B). *CCNE1* was neither a hotspot for TD formation in TDP tumors (see below) nor was it perturbed by the class 2 TDs characteristic of TDP group 2. In fact, only in 3% of *CCNE1* amplifications featured a class 2 TD. Importantly the significant association between *CCNE1* pathway activation and TDP status was maintained when those tumor samples where a class 2 TD duplicated the *CCNE1* gene were removed from the analysis (Table S4), supporting the hypothesis that *CCNE1* activation is a cause rather than a consequence of the TDP group 2 configuration.

TD Breakpoint Hotspots

We hypothesized that certain genomic loci may be targeted for TD formation and that these loci would differ across different TDPs. To address this possibility, we counted the number of TD breakpoints falling into consecutive 500-kb genomic windows for each one of the four major sets of TDs observed across the pan-cancer dataset (i.e., class 1 TDs [~ 11 kb], class 2 TDs [~ 231 kb], class 3 TDs (~ 1.7 Mb), and non-TDP TDs; Figure S4A). We then identified genomic hotspots as 500-kb windows with an observed number of breakpoints significantly larger than expected (see the STAR Methods). A total of 245 genomic windows were identified as genomic hotspots for TD breakpoints (Table S7). Importantly, the overall genomic distribution of the significant hotspots was very different when comparing the four TD classes. Most of the 101 genomic hotspots relative to the non-TDP TD breakpoints tightly clustered across a small number of distinct genomic regions that have been reported to be frequently involved in oncogene amplification (i.e., *ERBB2*, *MYC*, *CCND1*, *CDK4*, and *MDM2*; Figures 4A, S4B, and S4C). This confirms our previous report that TDs are commonly implicated in nucleating amplicon formation in regions of gene amplification in cancer (Inaki et al., 2014). By contrast, the TDP genomic hotspots were more uniformly scattered along the

genome (Figures 4B and S4C) and they appeared to engage different sets of oncogenic elements, with tumor suppressor genes (TSGs) and oncogenes being commonly found within the genomic hotspots identified for class 1 and class 2 TDs, respectively (Figure 4B and see below).

Of note, despite the fact that the number of class 1 TDs was more than double that of class 2 TDs (22,447 class 1 TDs versus 9,794 class 2 TDs), there was a larger number of class 2 TD breakpoint hotspots compared with class 1 (102 versus 30), suggesting greater selectivity for the formation of the short-span class 1 TDs (Figure S4B; Table S7).

Functional Consequences of TDPs: Gene Duplications and Gene Disruptions

We have previously shown that TDs occurring in the context of TDP are more likely to affect gene bodies of oncogenes and TSGs than what is expected by chance alone, suggesting a strong selection for consequential genomic "scars" that favor oncogenesis (Menghi et al., 2016). Herein, we extended our analysis to account for the effect of TDs of different span sizes (class 1 versus class 2 versus class 3), occurring across the distinct TDP groups. A TD can affect gene body integrity in one of three ways: (1) the TD spans the entire length of a gene body resulting in gene duplication; (2) both TD breakpoints fall within the gene body resulting in a disruptive double transection; and (3) only one TD breakpoint falls within a target gene body, resulting in a *de facto* gene copy-number neutral rearrangement. We posited that these effects would be systematically mediated by TDs of different span sizes, with larger TDs (>231 kb, i.e., class 2 and class 3) being mostly involved in gene duplications and shorter TDs (~ 11 kb, i.e., class 1) more frequently causing gene disruptions via double transections. In fact, we observed that 45% of class 1 TDs (Figure 5A) disrupt genes by double transection, but uncommonly result in single transections (18.2%) and even more rarely in gene duplications (5.7%), whereas the larger class 2 and class 3 TDs are more commonly implicated in single transections (66.9% and 74.7%, respectively) and in gene duplication (63.3% and 97.2%; Figure 5A). Importantly, these observations suggest that, by virtue of the nature of the prevalent TDs in each TDP group, distinct TDP subgroups are subjected to different forms of gene perturbation. Indeed, we found that TDP tumors featuring a prominent class 1 TD modal peak (i.e., TDP groups 1, 1/2mix, and 1/3mix) share a larger number of gene disruptions due to double transections as opposed to the other TDP tumors (Figure 5B). Conversely, TDP tumors with larger TD peaks (e.g., groups 2, 3, and 2/3mix) feature a significantly higher number of gene duplication events (Figure 5C).

Given our observation that TSGs and oncogenes preferentially map to breakpoint hotspot regions associated with short (class 1) and larger (class 2) TDs, respectively, we predicted that these two classes of cancer genes would be directly altered by TDs in ways that augment oncogenicity. To test this hypothesis, we analyzed which types of genes are affected by TDs more frequently than expected by chance alone (see the STAR Methods). We found that double transections, most commonly induced by class 1 TDs, predominantly and significantly disrupt TSGs, whereas gene duplications, which result from class 2 and class 3 TDs, predominantly engage oncogenes but not TSGs

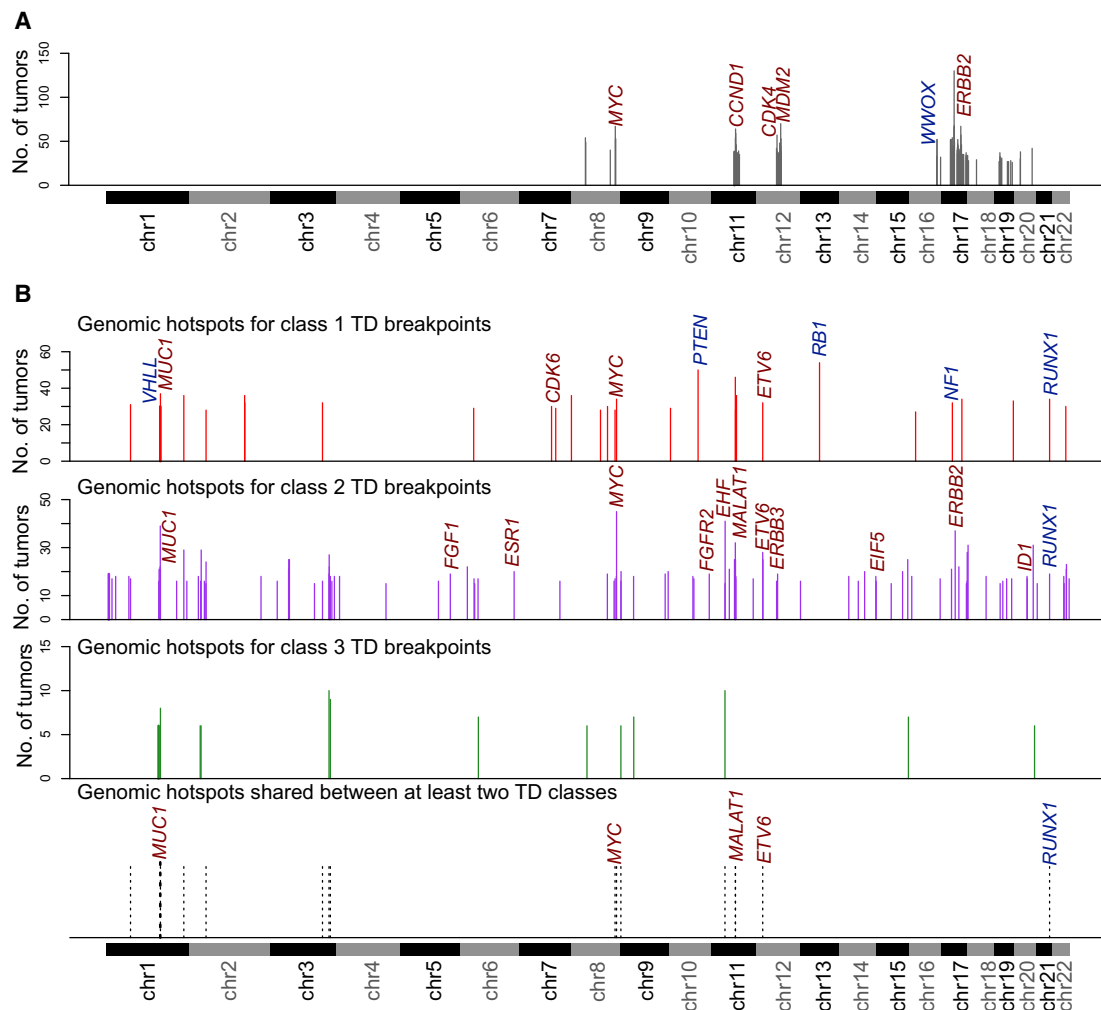


Figure 4. Genomic Hotspots of TD Breakpoints

(A) Genomic distribution of hotspots for TD breakpoints found in non-TDP tumors.

(B) Genomic distribution of hotspots for TD breakpoints found in TDP tumors. Top three panels: genomic hotspots for class 1, class 2, and class 3 TDs. Lower panel: recurrent genomic hotspots across different TD classes. Known oncogenes and TSGs are flagged in red and blue, respectively.

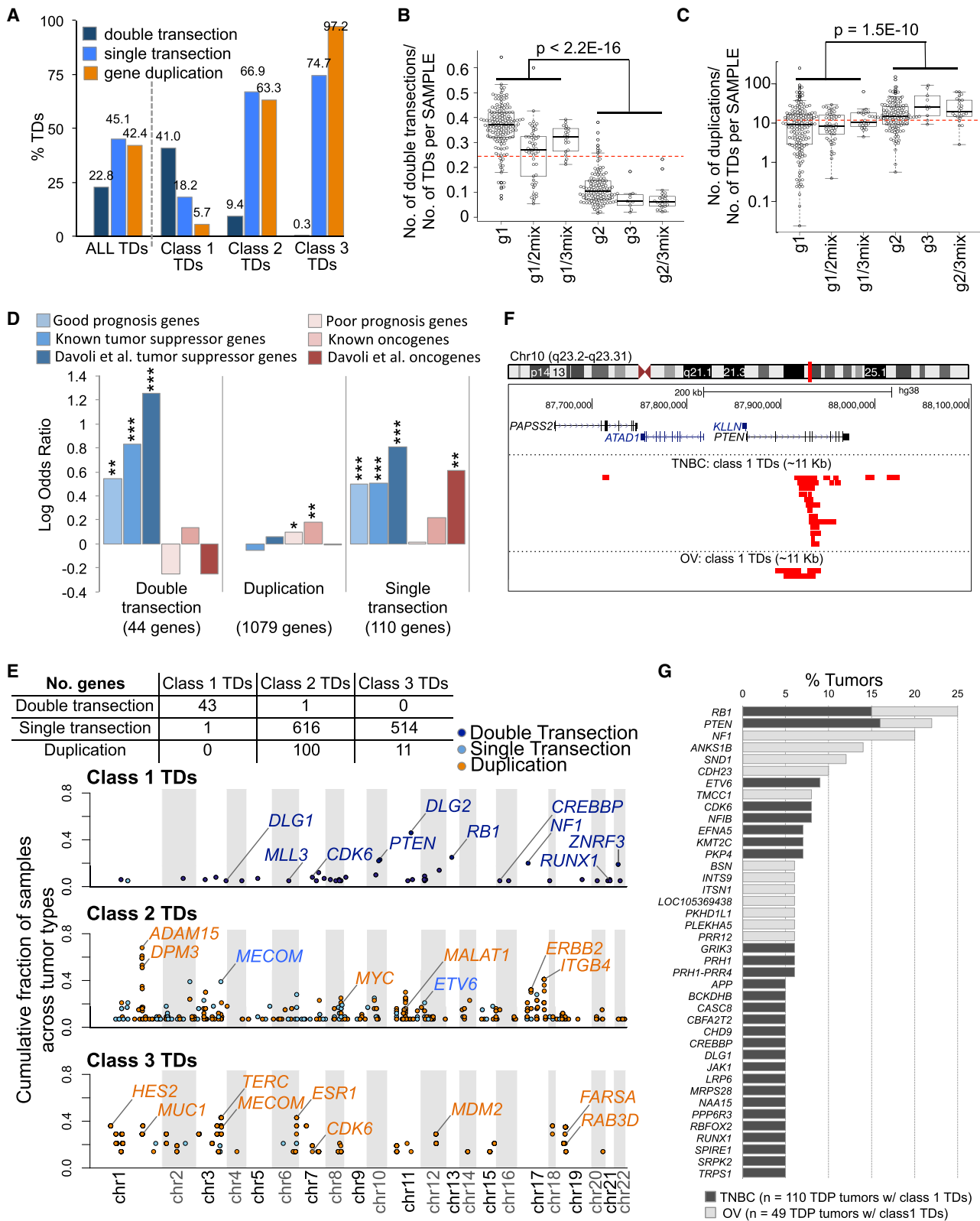
See also Table S7 and Figure S4.

(Figures 5D and 5E). Genes undergoing single transections should theoretically result in functionally neutral events: one allele transected but compensated by the duplication *in situ*. However, there was primarily an enrichment of TSGs at the sites of the single transections (Figure 5D). Though the precise mechanism is unclear, it is possible that the intact duplicated allele has been perturbed by either methylation, or by perturbation of specific regulatory elements, rendering the cell haplo-insufficient for the involved gene.

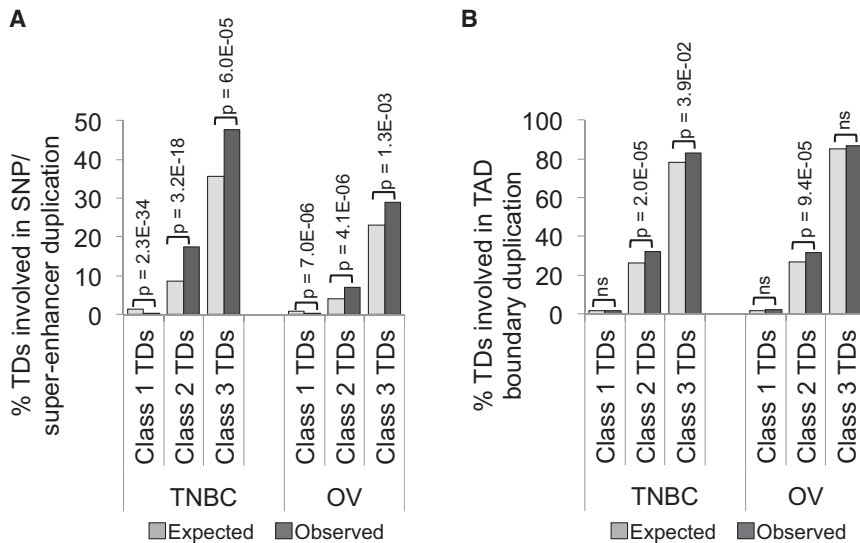
Among the most commonly disrupted TSGs were *PTEN* (affected in 16% and 6% of TNBC and OV TDPs with class 1 TDs), *RB1* (15% and 10% of TNBC and OV TDPs class 1 TDs), and *NF1* (20% of OV TDPs with class 1 TDs) (Figures 5E–G and S5; Table S8). In the majority of the cases we examined, these highly recurrent and potentially oncogenic TD-mediated events appeared to occur independently from each other (Figures S5A and S5B). Of note, given the strong causality between

loss of *BRCA1* and the presence of class 1 TDs, a *BRCA1*-null status is also significantly associated with disruption of the *PTEN*, *RB1*, and *NF1* genes via TD-mediated double transection in tumor samples that harbor wild-type exonic sequences for these genes (Figures S5A and S5B). This has implications for the clinical setting since this TD-mediated TSG disruption would not be detected using standard exome sequencing protocols (discussed below).

Genes that were recurrently duplicated by TDs included *ERBB2* (duplicated in 16% of UCEC, 9% of TNBC, and 7% of OV TDPs with class 2 TDs), *MYC* (21% of TNBC TDPs with class 2 TDs), and *ESR1* and *MDM2* (36% and 29%, of OV TDPs class 3 TDs, respectively) (Figures 5E and S5; Table S8). The oncogenic long non-coding RNA *MALAT1* was also often subjected to duplication in TNBC TDP tumors with class 2 TDs (12%), suggesting its activation by gene duplication (Figure S5A; Table S8).



(legend on next page)



Functional Consequences of TDPs: Duplication of Regulatory Elements and of Chromatin Structures

A recent study of breast cancer genomic rearrangements has found large span TDs (>100 kb) to frequently engage germline susceptibility loci and tissue-specific super-enhancers (Glodzik et al., 2017). Similarly, we found that cancer-associated SNPs identified by GWAS studies and tissue-specific super-enhancers are indeed commonly duplicated by large span TDs in TDP tumors. In TNBCs, both class 2 and class 3 TDs engage in the duplication of breast-specific regulatory elements more frequently than expected, based on 1,000 permutations of TD coordinates (Figure 6A; Table S9). Conversely, class 1 TDs are significantly less frequently involved in the duplication of these regulatory elements, even when considering their differential sequence spans (Figure 6A; Table S9).

Topologically associating domains (TADs) are conserved 3D chromatin-folding arrangements in the genome that facilitate coordinated transcriptional regulation. Perturbations of TAD structures are associated with transcriptional remodeling and alterations in transcriptional control (Dixon et al., 2012). This is especially true when TAD boundaries are disrupted and alternative/illegitimate enhancers are allowed to engage target gene promoters. We assessed whether TAD boundaries are disrupted

Figure 6. TD-Mediated Duplication of Tissue-Specific Regulatory Elements and TAD Boundaries in TDP Tumors

(A) Percentage of class 1, 2, and 3 TDs involved in the duplication of disease-associated SNPs and tissue-specific super-enhancers (observed versus expected) in the TNBC and OV datasets.

(B) Percentage of class 1, 2, and 3 TDs participating in TAD boundary duplication (observed versus expected) in the TNBC and OV datasets.

p values by chi-square test.

See also Table S6.

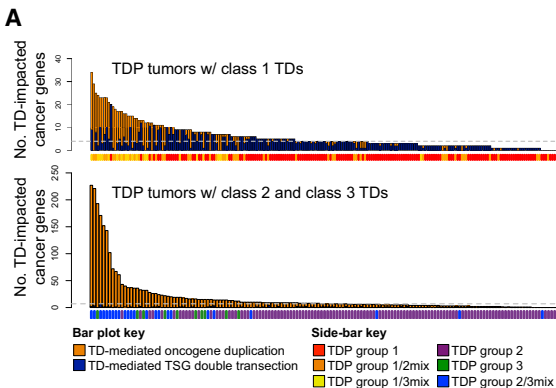
by TDs in TDP tumors. Specifically, we asked whether TAD boundaries are more likely to be duplicated by a TD in TNBC and, independently, in ovarian cancer. Using the CTCF-derived TAD genome map from the lymphoblastoid

cell line GM12878 as reference (Tang et al., 2015), we mapped TD coordinates to the 3D genome. We found that TAD boundaries are statistically more frequently duplicated than expected by chance alone by class 2 TDs in both the TNBC and OV datasets (Figure 6B; Table S9). By contrast only a very modest increase in TAD boundary duplications was seen for class 3 TDs in breast cancer, and no association at all was observed for class 1 TDs (Figure 6B).

Taken together, these analyses show that TDs in the context of TDP target many known oncogenic elements rather than concentrating on a few recurrent genes. On average, class 1 TDs found in TDP group 1 tumors result in the disruption of 3.7 known TSGs per genome but do not engage in the duplication of other oncogenic elements (Figures 7A and 7B). TDP group 1/2mix and TDP group 1/3mix have on average 2.6 disrupted TSGs, and 5.6 and 11.8 duplicated oncogenes, respectively (Figures 7A and 7B). By contrast, TDP groups 2, 3, and 2/3mix tumors that only feature larger span TDs rarely feature double transection of TSGs (on average 0.4, 0, and 1 TSG is affected in TDP groups 2, 3, and 2/3mix, respectively), but they feature a higher number of duplications, with an average of 6.8, 37.4, and 63 duplicated oncogenes per cancer genome, respectively (Figures 7A and 7B).

Figure 5. TD-Mediated Effects on Gene Bodies

- (A) Number of gene double and single transections and gene duplications caused by TDs of different span sizes.
 - (B) Number of TD-mediated gene double transections in TDP tumors with class 1 TDs (TDP groups 1, 1/2mix, and 1/3mix) compared with the other TDP tumors. Boxes span the interquartile range, with the median values marked by a horizontal line inside the box. Whiskers extend to 1.5 times the interquartile range from each box. p values by Mann-Whitney U test.
 - (C) Number of TD-mediated gene duplications in TDP tumors with a prevalence of class 2 and class 3 TDs (TDP groups 2, 3, and 2/3mix) compared with the other TDP tumors. Boxes span the interquartile range, with the median values marked by a horizontal line inside the box. Whiskers extend to 1.5 times the interquartile range from each box. p values by Mann-Whitney U test.
 - (D) TSG and oncogene enrichment across sets of genes recurrently impacted by TDs via single or double transection or duplication. ***p < 0.001, **p < 0.01, *p < 0.05, by Fisher's exact test.
 - (E) Recurrently TD-impacted genes by TD class and type of TD-mediated effect. Top: number of genes recurrently impacted by TDs in TDP tumors. Bottom: prevalence of TD-mediated gene disruptions: x_axis, genomic location; y_axis, cumulative fraction of affected TDP tumors across the different tumor types examined. Selected genes are flagged for easy of reference.
 - (F) High density of class 1 TDs at the PTEN locus in both the TNBC and OV datasets.
 - (G) Percentage of TDP tumors affected by significantly recurrent class 1 TD-mediated double transection events across the TNBC and OV datasets.
- See also Table S8 and Figure S5.



DISCUSSION

Herein, we provide a detailed analysis of one cancer chromotype, the TDP, by devising a simple quantitative scoring system to better defining TDP taxonomy. We showed that TDPs can be classified by the predominant span size of their TDs: 11 kb (i.e., class 1), 231 kb (i.e., class 2), and 1.7 Mb (i.e., class 3). This subclassification was the key to identify the primary drivers of genome-wide TD formation. Of all TDP tumors, those characterized by class 1 TDs, alone (i.e., TDP group 1) or in combination with other TD span sizes (i.e., TDP groups 1/2mix and 1/3mix) were significantly enriched for the conjoint loss of BRCA1 and p53. We proved the genesis of the TDP group 1 configuration in murine models of mammary cancers driven by the homozygous deletion of *Trp53* and *Brca1*, suggesting that perturbation of BRCA1 has universal genome-wide effects distinct from BRCA2.

In support of this model, we have recently defined the mechanism of TD formation in murine embryonic stem cell (ESC) cultures, where TDs form at sites of replication fork stalling in *Brca1*-depleted cells by a mechanism that entails re-replication of kilobases-long tracts of chromosomal DNA adjacent to the site of fork stalling (Willis et al., 2017). This effect was also specific to BRCA1 loss and was not a feature of BRCA2 loss. The striking similarities between the genetic control of TD formation in this model and the induction of TDP group 1 tumors strongly suggest that class 1 TDs in cancer arise by similar aberrant re-replication at stalled forks exclusively in the presence of defective activity of the BRCA1 protein. Though *Trp53* was not genetically disrupted in the ESC culture model, it is known that the p53 protein in mouse ESCs does not translocate to the nucleus in response to DNA damage to activate a p53-dependent response (Aladjem et al., 1998). Thus, mouse ESCs are functionally deficient in p53, closely resembling the *TP53* null condition identified in TDP tumors. Precisely how loss of BRCA1 “licenses” class 1 TD formation and why BRCA2 does not is currently unknown. In this regard, although BRCA1 and BRCA2 have common roles in regulating RAD51-mediated homologous recombination (HR) and at stalled forks, BRCA1 has additional functions in double-strand break (DSB) repair and in stalled fork metabolism that are not shared with BRCA2 (Aladjem et al., 1998; Pathania et al., 2011; Prakash et al., 2015; Schlacher et al., 2012).

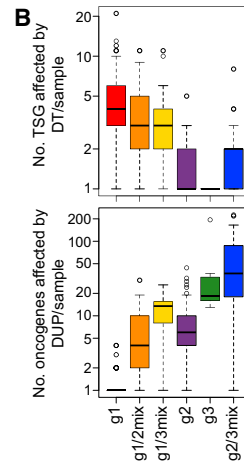


Figure 7. Number of TD-Mediated TSG Disruptions and Oncogene Duplications across Different TDP Groups

(A) Number of known cancer genes per genome that are duplicated or disrupted as a result of specific TDP configurations.

(B) Boxplot summary of the data presented in (A). Boxes span the interquartile range, with the median values marked by a horizontal line inside the box. Whiskers extend to 1.5 times the interquartile range from each box, and outliers are drawn as individual points extending past the whiskers.

The genetic origins of the BRCA1-proficient TDP subgroups (groups 2, 3, and 2/3mix), characterized by larger class 2 (~231 kb), and/or class 3 (~1.7 Mb) TDs,

are more heterogeneous. By association, we found that activation of the CCNE1 pathway either through CCNE1 amplification or by *FBXW7* mutation accounted for 40% of TDP group 2 tumors across each one of the TNBC, OV, and UCEC datasets, but only manifested in 10% of non-TDP and <3% TDP group 1 tumors. CCNE1 is known to engage cyclin-dependent kinases to regulate cell-cycle progression. Its deregulation causes replicative stress by slowing replication fork progression, reducing intracellular nucleotide pools (Bester et al., 2011), and inducing cells to enter into mitosis with short incompletely replicated genomic segments (Teixeira et al., 2015). As a model of oncogene-induced replicative stress, CCNE1 overexpression in U2OS cells induced copy-number alterations, which were predominantly segmental duplications (Costantino et al., 2014).

Somatic mutations affecting CDK12 were most prevalent in TDP group 2/3mix tumors, which comprise both class 2 and class 3 TDs, indicating a mechanism of TD formation distinct from the augmented CCNE1 function hypothesized for TDP group 2 tumors. CDK12 is an RNA polymerase II C-terminal domain kinase that transcriptionally regulates several HR genes. Defects in CDK12 are associated with the downregulation of critical regulators of genomic stability such as *BRCA1*, *ATR*, *FANCI*, and *FANCD2* (Blazek et al., 2011; Joshi et al., 2014). That loss of CDK12 affects *BRCA1* expression but generates a TDP profile that is clearly distinct from the BRCA1-dependent TDP group 1 configuration suggests that the primary action of CDK12 is likely to be different from its effects on *BRCA1*.

The TDP is a model for combinatorial genetics in cancer. By classifying the effect of TDs on gene bodies, we showed that the TDP generates a genome-scale pro-oncogenic configuration resulting from the modulation of tens of potential oncogenic signals. These effects were mediated systematically by TDs of different span sizes, with larger TDs (class 2 and class 3, >231 kb) being mostly involved in the duplication of oncogenes and regulatory elements and TAD disruption, and shorter TDs (class 1, ~11 kb) more frequently causing TSG disruptions.

The top three genes disrupted by class 1 TDs were *PTEN* and *RB1* in both TNBC and OV cancer types and *NF1* in the OV dataset. These genes are predominantly implicated in cell survival and cell-cycle regulation through the PI3K, E2F, and RAS pathways. However, recent evidence showed a role for their products

in modulating genetic instability. RB1 has been reported to be essential for DNA DSB repair by canonical non-homologous end joining, a defect invoked to explain the high incidence of genomic instability in RB1-mutant cancers (Cook et al., 2015). PTEN has been considered a major factor in genome stability through its effects on maintaining centromere stability, by controlling RAD51 expression (Shen et al., 2007), and by recruitment of RAD51 through physical association of PTEN with DNA replication forks. These studies suggest a function for PTEN with RAD51 in promoting the restart at stalled replication forks (He et al., 2015). The role of NF1 in HR-deficient tumors, although statistically observed, is less established. However, the C3H-Mcm4Chaos3/Chaos3 mouse model, which harbors a disruption of *Mcm4* (encoding a member of the family of MCM2–7 replicative helicases), invariably results in mammary cancers with *Nf1* deletions and chromosomal instability (Wallace et al., 2012). Thus, TDP groups 1, 1/2mix, and 1/3mix tumors, which originate with defects in BRCA1-mediated HR mechanisms, appear to compound the defect by accumulating downstream mutations that disable genes involved in chromosomal stability and DNA repair, in addition to cellular functions such as cell-cycle and cellular metabolism. By contrast, TDP groups 2, 2/3mix, and 3 tumors recurrently duplicate oncogenes such as *MYC* and *ERBB2*, oncogenic lncRNAs such as *MALAT1*, and disrupt TADs. This would suggest that, although the genomic characteristic is TD formation, the functional consequences of TD-induced abnormalities vary significantly between the TDP forms.

Taken together, our data suggest a mechanistic scenario for TDP induction, where specific HR defects (e.g., loss of BRCA1 or CDK12, but not of BRCA2) and excessive replicative stress (CCNE1 pathway activation) in the presence of replication fork stalling enhance TD formation. In 91% (151/166) of TDP cancers with full genomic mutational ascertainment definitively involving one of these three driver genes, we observed concomitant mutation of *TP53*, implying that defective DNA damage checkpoint control facilitated tumorigenesis, TD formation, or both. Although disruptions of each of these genes have in the past been implicated in general genomic instability, our findings reveal that these oncogenic drivers induce a much more specific pattern of structural rearrangements (i.e., the TDP) than was previously suspected.

The analysis of the gene disruptions as a consequence of TDP raises other therapeutic possibilities. Potentially disruptive double transections of *PTEN* were found in 16% of TNBCs with class 1 TDs. *PTEN* knockout cells were preferentially sensitive to PARP inhibitors in a synthetic lethal screen (Mendes-Pereira et al., 2009) suggesting that TDPs with *PTEN* disruptions may have greater deficiencies in DNA repair and may be more sensitive to a range of agents that include cisplatin and PARP inhibitors. In fact, the number of known cancer genes affected by TDs ranged from an average of ~4 (in TDP group 1) to ~60 (in TDP group 2/3mix), suggesting that the TDP is a state where the mutational combinatorics can generate a range of potential therapeutic modifiers, some of which may be exploited to enhance treatment efficacy.

Our results provide a detailed view of a specific chromosomal configuration in cancer characterized by genetically distributed TDs that unifies a number of reports focused on individual cancer types. We show that conjoint *BRCA1* and *TP53* mutations are

essential to forming a precise TDP state that features short-span TDs. Additional studies should further delineate the mechanisms of the other forms of TDP formation, and answer why their associated TDs are restricted to specific size ranges.

STAR METHODS

Detailed methods are provided in the online version of this paper and include the following:

- KEY RESOURCES TABLE
- CONTACT FOR REAGENT AND RESOURCE SHARING
- EXPERIMENTAL MODEL AND SUBJECT DETAILS
 - PDXs
 - Mouse Models of Breast Cancer
- METHOD DETAILS
 - Data Collection for TDP Classification
 - TCGA Cohort Data Collection and Processing
 - Other Publicly Available WGS Cancer Cohorts
 - In-House WGS Cohort and Mouse Tumor Sequencing
 - The TDP Classification Algorithm
 - SNV Association Analysis
 - CNV Association Analysis
 - TD Breakpoint Analysis
 - Analysis of Recurrently TD-Impacted Genes
 - Cancer Gene Lists
 - Analysis of Disease-Associated Single Nucleotide Polymorphisms (SNPs) and Tissue-Specific Super-Enhancers
 - Analysis of Topologically Associating Domains (TADs)
- DATA AND SOFTWARE AVAILABILITY
- QUANTIFICATION AND STATISTICAL ANALYSIS

SUPPLEMENTAL INFORMATION

Supplemental Information includes five figures and nine tables and can be found with this article online at <https://doi.org/10.1016/j.ccr.2018.06.008>.

ACKNOWLEDGMENTS

WGS library preparation, sequencing and analysis were performed by JAX Cancer Center Shared Resources (Genomic Technology and the Computational Sciences) at The Jackson Laboratory for Genomic Medicine, CT 06030, USA. This work was supported by NCI grant P30CA034196 (to E.T.L.), DoD CDMRP grants W81XWH-17-1-0005 (to E.T.L.) and W81XWH-17-1-0006 (to R.S.), the Andrea Branch and David Elliman Cancer Study Fund and the Scott R. MacKenzie Foundation (to E.T.L.), NIH grant R01CA190121 (to R.G.W.V.), CPRIT grant R140606 (to R.G.W.V.), NWO/ZonMW Vici grant 918.146.43 (to J.J.), ERC Synergy grant 319661 (to J.J.), Cancer Genomics Netherlands (to J.J.), and the OncoCode Institute co-financed by the Dutch Cancer Society (to J.J.). B.J. was partially funded by the Gil Ehrlich Foundation.

AUTHOR CONTRIBUTIONS

Conceptualization, F.M. and E.T.L.; Methodology, F.M. and E.T.L.; Software and Formal Analysis: F.M., F.P.B., V.Y., M.T., B.J., and Z.T.; Investigation, F.M., V.Y., B.J., and Z.T.; Writing – Original Draft, F.M. and E.T.L.; Writing – Review & Editing, F.M. and E.T.L., F.P.B., B.J., Z.T., G.W.C., and R.S.; Funding Acquisition, F.M. and E.T.L.; Resources, J.J.; Supervision, E.T.L., G.W.C., Y.R., R.S., and R.G.W.V.

DECLARATION OF INTERESTS

The authors declare no competing interests.

Received: January 15, 2018

Revised: May 4, 2018

Accepted: June 14, 2018

Published: July 12, 2018

REFERENCES

- Aladjem, M.I., Spike, B.T., Rodewald, L.W., Hope, T.J., Klemm, M., Jaenisch, R., and Wahl, G.M. (1998). ES cells do not activate p53-dependent stress responses and undergo p53-independent apoptosis in response to DNA damage. *Curr. Biol.* 8, 145–155.
- Baca, S.C., Prandi, D., Lawrence, M.S., Mosquera, J.M., Romanel, A., Drier, Y., Park, K., Kitabayashi, N., MacDonald, T.Y., Ghani, M., et al. (2013). Punctuated evolution of prostate cancer genomes. *Cell* 153, 666–677.
- Bailey, P., Chang, D.K., Nones, K., Johns, A.L., Patch, A.M., Gingras, M.C., Miller, D.K., Christ, A.N., Bruxner, T.J., Quinn, M.C., et al. (2016). Genomic analyses identify molecular subtypes of pancreatic cancer. *Nature* 531, 47–52.
- Barthel, F.P., Wei, W., Tang, M., Martinez-Ledesma, E., Hu, X., Amin, S.B., Akdemir, K.C., Seth, S., Song, X., Wang, Q., et al. (2017). Systematic analysis of telomere length and somatic alterations in 31 cancer types. *Nat. Genet.* 49, 349–357.
- Bass, A.J., Lawrence, M.S., Brace, L.E., Ramos, A.H., Drier, Y., Cibulskis, K., Sougnez, C., Voet, D., Saksena, G., Sivachenko, A., et al. (2011). Genomic sequencing of colorectal adenocarcinomas identifies a recurrent VTI1A-TCF7L2 fusion. *Nat. Genet.* 43, 964–968.
- Berger, M.F., Hodis, E., Heffernan, T.P., Deribe, Y.L., Lawrence, M.S., Protopopov, A., Ivanova, E., Watson, I.R., Nickerson, E., Ghosh, P., et al. (2012). Melanoma genome sequencing reveals frequent PREX2 mutations. *Nature* 485, 502–506.
- Berger, M.F., Lawrence, M.S., Demichelis, F., Drier, Y., Cibulskis, K., Sivachenko, A.Y., Sboner, A., Esgueva, R., Pflueger, D., Sougnez, C., et al. (2011). The genomic complexity of primary human prostate cancer. *Nature* 470, 214–220.
- Bester, A.C., Roniger, M., Oren, Y.S., Im, M.M., Sarni, D., Chaoat, M., Bensimon, A., Zamir, G., Shewach, D.S., and Kerem, B. (2011). Nucleotide deficiency promotes genomic instability in early stages of cancer development. *Cell* 145, 435–446.
- Blazek, D., Kohoutek, J., Bartholomeeusen, K., Johansen, E., Hulinkova, P., Luo, Z., Cimermancic, P., Ule, J., and Peterlin, B.M. (2011). The cyclin K/Cdk12 complex maintains genomic stability via regulation of expression of DNA damage response genes. *Genes Dev.* 25, 2158–2172.
- Campbell, P.J., Yachida, S., Mudie, L.J., Stephens, P.J., Pleasance, E.D., Stebbings, L.A., Morsberger, L.A., Latimer, C., McLaren, S., Lin, M.L., et al. (2010). The patterns and dynamics of genomic instability in metastatic pancreatic cancer. *Nature* 467, 1109–1113.
- Cancer Genome Atlas Research Network, Kandoth, C., Schultz, N., Cherniack, A.D., Akbani, R., Liu, Y., Shen, H., Robertson, A.G., Pashtan, I., Shen, R., Benz, C.C., et al. (2013). Integrated genomic characterization of endometrial carcinoma. *Nature* 497, 67–73.
- Chen, K., Wallis, J.W., McLellan, M.D., Larson, D.E., Kalicki, J.M., Pohl, C.S., McGrath, S.D., Wendl, M.C., Zhang, Q., Locke, D.P., et al. (2009). BreakDancer: an algorithm for high-resolution mapping of genomic structural variation. *Nat. Methods* 6, 677–681.
- Chiang, C., Layer, R.M., Faust, G.G., Lindberg, M.R., Rose, D.B., Garrison, E.P., Marth, G.T., Quinlan, A.R., and Hall, I.M. (2015). SpeedSeq: ultra-fast personal genome analysis and interpretation. *Nat. Methods* 12, 966–968.
- Connor, A.A., Denroche, R.E., Jang, G.H., Timms, L., Kalimuthu, S.N., Selander, I., McPherson, T., Wilson, G.W., Chan-Seng-Yue, M.A., Borozan, I., et al. (2017). Association of distinct mutational signatures with correlates of increased immune activity in pancreatic ductal adenocarcinoma. *JAMA Oncol.* 3, 774–783.
- Conway, T., Wazny, J., Bromage, A., Tymms, M., Sooraj, D., Williams, E.D., and Beresford-Smith, B. (2012). Xenome – a tool for classifying reads from xenograft samples. *Bioinformatics* 28, i172–i178.
- Cook, R., Zoumpoulidou, G., Luczynski, M.T., Rieger, S., Moquet, J., Spanswick, V.J., Hartley, J.A., Rothkamm, K., Huang, P.H., and Mittnacht, S. (2015). Direct involvement of retinoblastoma family proteins in DNA repair by non-homologous end-joining. *Cell Rep.* 10, 2006–2018.
- Costantino, L., Sotiriou, S.K., Rantala, J.K., Magin, S., Mladenov, E., Helleday, T., Haber, J.E., Iliakis, G., Kallioniemi, O.P., and Halazonetis, T.D. (2014). Break-induced replication repair of damaged forks induces genomic duplications in human cells. *Science* 343, 88–91.
- Davoli, T., Xu, A.W., Mengwasser, K.E., Sack, L.M., Yoon, J.C., Park, P.J., and Elledge, S.J. (2013). Cumulative haploinsufficiency and triplosensitivity drive aneuploidy patterns and shape the cancer genome. *Cell* 155, 948–962.
- Desmedt, C., Fumagalli, D., Pietri, E., Zoppoli, G., Brown, D., Nik-Zainal, S., Gundem, G., Rothe, F., Majaj, S., Garuti, A., et al. (2015). Uncovering the genomic heterogeneity of multifocal breast cancer. *J. Pathol.* 236, 457–466.
- Dixon, J.R., Selvaraj, S., Yue, F., Kim, A., Li, Y., Shen, Y., Hu, M., Liu, J.S., and Ren, B. (2012). Topological domains in mammalian genomes identified by analysis of chromatin interactions. *Nature* 485, 376–380.
- Etemadmoghadam, D., Weir, B.A., Au-Yeung, G., Alsop, K., Mitchell, G., George, J., Australian Ovarian Cancer Study, G., Davis, S., D'Andrea, A.D., Simpson, K., et al. (2013). Synthetic lethality between CCNE1 amplification and loss of BRCA1. *Proc. Natl. Acad. Sci. USA* 110, 19489–19494.
- Ferrari, A., Vincent-Salomon, A., Pivot, X., Sertier, A.S., Thomas, E., Tonon, L., Boyault, S., Mulugeta, E., Treilleux, I., MacGrogan, G., et al. (2016). A whole-genome sequence and transcriptome perspective on HER2-positive breast cancers. *Nat. Commun.* 7, 12222.
- Fujimoto, A., Furuta, M., Totoki, Y., Tsunoda, T., Kato, M., Shiraishi, Y., Tanaka, H., Taniguchi, H., Kawakami, Y., Ueno, M., et al. (2016). Whole-genome mutational landscape and characterization of noncoding and structural mutations in liver cancer. *Nat. Genet.* 48, 500–509.
- Glodzik, D., Morganella, S., Davies, H., Simpson, P.T., Li, Y., Zou, X., Diez-Perez, J., Staaf, J., Alexandrov, L.B., Smid, M., et al. (2017). A somatic-mutational process recurrently duplicates germline susceptibility loci and tissue-specific super-enhancers in breast cancers. *Nat. Genet.* 49, 341–348.
- Grzeda, K.R., Royer-Bertrand, B., Inaki, K., Kim, H., Hillmer, A.M., Liu, E.T., and Chuang, J.H. (2014). Functional chromatin features are associated with structural mutations in cancer. *BMC Genomics* 15, 1013.
- He, J., Kang, X., Yin, Y., Chao, K.S., and Shen, W.H. (2015). PTEN regulates DNA replication progression and stalled fork recovery. *Nat. Commun.* 6, 7620.
- Hillmer, A.M., Yao, F., Inaki, K., Lee, W.H., Ariyaratne, P.N., Teo, A.S., Woo, X.Y., Zhang, Z., Zhao, H., Ukil, L., et al. (2011). Comprehensive long-span paired-end-tag mapping reveals characteristic patterns of structural variations in epithelial cancer genomes. *Genome Res.* 21, 665–675.
- Hnisz, D., Abraham, B.J., Lee, T.I., Lau, A., Saint-Andre, V., Sigova, A.A., Hoke, H.A., and Young, R.A. (2013). Super-enhancers in the control of cell identity and disease. *Cell* 155, 934–947.
- Imielinski, M., Berger, A.H., Hammerman, P.S., Hernandez, B., Pugh, T.J., Hodis, E., Cho, J., Suh, J., Capelletti, M., Sivachenko, A., et al. (2012). Mapping the hallmarks of lung adenocarcinoma with massively parallel sequencing. *Cell* 150, 1107–1120.
- Inaki, K., Menghi, F., Woo, X.Y., Wagner, J.P., Jacques, P.E., Lee, Y.F., Shreckengast, P.T., Soon, W.W., Malhotra, A., Teo, A.S., et al. (2014). Systems consequences of amplicon formation in human breast cancer. *Genome Res.* 24, 1559–1571.
- Jonkers, J., Meuwissen, R., van der Gulden, H., Peterse, H., van der Valk, M., and Berns, A. (2001). Synergistic tumor suppressor activity of BRCA2 and p53 in a conditional mouse model for breast cancer. *Nat. Genet.* 29, 418–425.
- Joshi, P.M., Sutor, S.L., Huntoon, C.J., and Karnitz, L.M. (2014). Ovarian cancer-associated mutations disable catalytic activity of CDK12, a kinase that promotes homologous recombination repair and resistance to cisplatin and poly(ADP-ribose) polymerase inhibitors. *J. Biol. Chem.* 289, 9247–9253.

- Kataoka, K., Nagata, Y., Kitanaka, A., Shiraishi, Y., Shimamura, T., Yasunaga, J., Totoki, Y., Chiba, K., Sato-Otsubo, A., Nagae, G., et al. (2015). Integrated molecular analysis of adult T cell leukemia/lymphoma. *Nat. Genet.* 47, 1304–1315.
- Klotz, K., Cepeda, D., Tan, Y., Sun, D., Sangfelt, O., and Spruck, C. (2009). SCF(Fbxw7/hCdc4) targets cyclin E2 for ubiquitin-dependent proteolysis. *Exp. Cell Res.* 315, 1832–1839.
- Kuznetsova, A., Brockhoff, P.B., and Christensen, R.H.B. (2017). ImerTest package: tests in linear mixed effects models. *J. Stat. Softw.* 82, 1–26.
- Lindberg, M.R., Hall, I.M., and Quinlan, A.R. (2015). Population-based structural variation discovery with Hydra-Multi. *Bioinformatics* 31, 1286–1289.
- Liu, X., Holstege, H., van der Gulden, H., Treur-Mulder, M., Zevenhoven, J., Velds, A., Kerkhoven, R.M., van Vliet, M.H., Wessels, L.F., Peterse, J.L., et al. (2007). Somatic loss of BRCA1 and p53 in mice induces mammary tumors with features of human BRCA1-mutated basal-like breast cancer. *Proc. Natl. Acad. Sci. USA* 104, 12111–12116.
- McBride, D.J., Etemadmoghadam, D., Cooke, S.L., Alsop, K., George, J., Butler, A., Cho, J., Galappaththige, D., Greenman, C., Howarth, K.D., et al. (2012). Tandem duplication of chromosomal segments is common in ovarian and breast cancer genomes. *J. Pathol.* 227, 446–455.
- Mendes-Pereira, A.M., Martin, S.A., Brough, R., McCarthy, A., Taylor, J.R., Kim, J.S., Waldman, T., Lord, C.J., and Ashworth, A. (2009). Synthetic lethal targeting of PTEN mutant cells with PARP inhibitors. *EMBO Mol. Med.* 1, 315–322.
- Menghi, F., Inaki, K., Woo, X., Kumar, P.A., Grzeda, K.R., Malhotra, A., Yadav, V., Kim, H., Marquez, E.J., Ucar, D., et al. (2016). The tandem duplicator phenotype as a distinct genomic configuration in cancer. *Proc. Natl. Acad. Sci. USA* 113, E2373–E2382.
- Menghi, F., and Liu, E.T. (2016). Reply to Watkins et al.: whole-genome sequencing-based identification of diverse tandem duplicator phenotypes in human cancers. *Proc. Natl. Acad. Sci. USA* 113, E5259–E5260.
- Natrajan, R., Mackay, A., Lambros, M.B., Weigelt, B., Wilkerson, P.M., Manie, E., Grigoriadis, A., A'Hern, R., van der Groep, P., Kozarewa, I., et al. (2012). A whole-genome massively parallel sequencing analysis of BRCA1 mutant oestrogen receptor-negative and -positive breast cancers. *J. Pathol.* 227, 29–41.
- Ng, C.K., Cooke, S.L., Howe, K., Newman, S., Xian, J., Temple, J., Batty, E.M., Pole, J.C., Langdon, S.P., Edwards, P.A., and Brenton, J.D. (2012). The role of tandem duplicator phenotype in tumour evolution in high-grade serous ovarian cancer. *J. Pathol.* 226, 703–712.
- Nik-Zainal, S., Alexandrov, L.B., Wedge, D.C., Van Loo, P., Greenman, C.D., Raine, K., Jones, D., Hinton, J., Marshall, J., Stebbings, L.A., et al. (2012). Mutational processes molding the genomes of 21 breast cancers. *Cell* 149, 979–993.
- Nik-Zainal, S., Davies, H., Staaf, J., Ramakrishna, M., Glodzik, D., Zou, X., Martincorena, I., Alexandrov, L.B., Martin, S., Wedge, D.C., et al. (2016). Landscape of somatic mutations in 560 breast cancer whole-genome sequences. *Nature* 534, 47–54.
- Northcott, P.A., Shih, D.J., Peacock, J., Garzia, L., Morrissey, A.S., Zichner, T., Stutz, A.M., Korshunov, A., Reimand, J., Schumacher, S.E., et al. (2012). Subgroup-specific structural variation across 1,000 medulloblastoma genomes. *Nature* 488, 49–56.
- Patch, A.M., Christie, E.L., Etemadmoghadam, D., Garsed, D.W., George, J., Fereday, S., Nones, K., Cowin, P., Alsop, K., Bailey, P.J., et al. (2015). Whole-genome characterization of chemoresistant ovarian cancer. *Nature* 521, 489–494.
- Pathania, S., Nguyen, J., Hill, S.J., Scully, R., Adelman, G.O., Marto, J.A., Feunteun, J., and Livingston, D.M. (2011). BRCA1 is required for postreplication repair after UV-induced DNA damage. *Mol. Cell* 44, 235–251.
- Pinto, E.M., Chen, X., Easton, J., Finkelstein, D., Liu, Z., Pounds, S., Rodriguez-Galindo, C., Lund, T.C., Mardis, E.R., Wilson, R.K., et al. (2015). Genomic landscape of paediatric adrenocortical tumours. *Nat. Commun.* 6, 6302.
- Popova, T., Manie, E., Boeva, V., Battistella, A., Goundiam, O., Smith, N.K., Mueller, C.R., Raynal, V., Mariani, O., Sastre-Garau, X., and Stern, M.H. (2016). Ovarian cancers harboring inactivating mutations in CDK12 display a distinct genomic instability pattern characterized by large tandem duplications. *Cancer Res.* 76, 1882–1891.
- Prakash, R., Zhang, Y., Feng, W., and Jasin, M. (2015). Homologous recombination and human health: the roles of BRCA1, BRCA2, and associated proteins. *Cold Spring Harb. Perspect. Biol.* 7, a016600.
- Rausch, T., Zichner, T., Schlattl, A., Stutz, A.M., Benes, V., and Korbel, J.O. (2012). DELLY: structural variant discovery by integrated paired-end and split-read analysis. *Bioinformatics* 28, i333–i339.
- Schlacher, K., Wu, H., and Jasin, M. (2012). A distinct replication fork protection pathway connects Fanconi anemia tumor suppressors to RAD51-BRCA1/2. *Cancer Cell* 22, 106–116.
- Shen, W.H., Balajee, A.S., Wang, J., Wu, H., Eng, C., Pandolfi, P.P., and Yin, Y. (2007). Essential role for nuclear PTEN in maintaining chromosomal integrity. *Cell* 128, 157–170.
- Stephens, P.J., Greenman, C.D., Fu, B., Yang, F., Bignell, G.R., Mudie, L.J., Pleasance, E.D., Lau, K.W., Beare, D., Stebbings, L.A., et al. (2011). Massive genomic rearrangement acquired in a single catastrophic event during cancer development. *Cell* 144, 27–40.
- Stephens, P.J., McBride, D.J., Lin, M.L., Varela, I., Pleasance, E.D., Simpson, J.T., Stebbings, L.A., Leroy, C., Edkins, S., Mudie, L.J., et al. (2009). Complex landscapes of somatic rearrangement in human breast cancer genomes. *Nature* 462, 1005–1010.
- Tang, Z., Luo, O.J., Li, X., Zheng, M., Zhu, J.J., Szalaj, P., Trzaskoma, P., Magalska, A., Włodarczyk, J., Ruszczycki, B., et al. (2015). CTCF-mediated human 3D genome architecture reveals chromatin topology for transcription. *Cell* 163, 1611–1627.
- Teixeira, L.K., Wang, X., Li, Y., Ekholm-Reed, S., Wu, X., Wang, P., and Reed, S.I. (2015). Cyclin E deregulation promotes loss of specific genomic regions. *Curr. Biol.* 25, 1327–1333.
- Totoki, Y., Yoshida, A., Hosoda, F., Nakamura, H., Hama, N., Ogura, K., Yoshida, A., Fujiwara, T., Arai, Y., Toguchida, J., et al. (2014). Unique mutation portraits and frequent COL2A1 gene alteration in chondrosarcoma. *Genome Res.* 24, 1411–1420.
- Wallace, M.D., Pfefferle, A.D., Shen, L., McNairn, A.J., Cerami, E.G., Fallon, B.L., Rinaldi, V.D., Southard, T.L., Perou, C.M., and Schimenti, J.C. (2012). Comparative oncogenomics implicates the neurofibromin 1 gene (NF1) as a breast cancer driver. *Genetics* 192, 385–396.
- Wang, J., Mullighan, C.G., Easton, J., Roberts, S., Heatley, S.L., Ma, J., Rusch, M.C., Chen, K., Harris, C.C., Ding, L., et al. (2011). CREST maps somatic structural variation in cancer genomes with base-pair resolution. *Nat. Methods* 8, 652–654.
- Willis, N.A., Frock, R.L., Menghi, F., Duffey, E.E., Panday, A., Camacho, V., Hasty, E.P., Liu, E.T., Alt, F.W., and Scully, R. (2017). Mechanism of tandem duplication formation in BRCA1-mutant cells. *Nature* 551, 590–595.
- Xi, R., Hadjipanayis, A.G., Luquette, L.J., Kim, T.M., Lee, E., Zhang, J., Johnson, M.D., Muzny, D.M., Wheeler, D.A., Gibbs, R.A., et al. (2011). Copy number variation detection in whole-genome sequencing data using the Bayesian information criterion. *Proc. Natl. Acad. Sci. USA* 108, E1128–E1136.
- Yang, L., Luquette, L.J., Gehlenborg, N., Xi, R., Haseley, P.S., Hsieh, C.H., Zhang, C., Ren, X., Protopopov, A., Chin, L., et al. (2013). Diverse mechanisms of somatic structural variations in human cancer genomes. *Cell* 153, 919–929.

STAR★METHODS**KEY RESOURCES TABLE**

REAGENT or RESOURCE	SOURCE	IDENTIFIER
Biological Samples		
Patient-derived xenografts (PDX)	The Jackson Laboratory	TM01079, TM00099, TM00089, TM00097, TM01117, TM00091, TM01278, TM00098, J000099327, TM00090, TM01273, TM00096, TM00999, J000080739, TM00093, TM00094
Deposited Data		
PDX WGS data	This paper	Sequence Read Archive database, SRA: PRJNA430898.
Mouse mammary tumor WGS data	This paper	Sequence Read Archive database, SRA: PRJNA430898.
TCGA WGS	Cancer Genomics Hub	https://cghub.ucsc.edu/
Genomic coordinates for GM12878 topologically associating domains (TADs)	Tang et al., 2015	N/A
Tissue-specific super-enhancers and disease-associated SNPs (breast and ovarian tissues)	Hnisz et al., 2013	N/A
TCGA gene-based copy number calls	UCSC Cancer Genomic Browser (https://genome-cancer.ucsc.edu)	TCGA_PANCAN_gistic2, version: 2015-02-06
Somatic single nucleotide variation (SNV) data	COSMIC data portal (http://cancer.sanger.ac.uk/cosmic)	Data freeze version v78
WGS-based somatic structural variation calls (set 1)	ICGC Data Portal (https://dcc.icgc.org/)	Data freeze version 22
WGS-based somatic structural variation calls (set 2)	COSMIC data portal (http://cancer.sanger.ac.uk/cosmic)	Data freeze version v78
Experimental Models: Organisms/Strains		
Mouse: KP: 129/Ola,FVB/N-K14cre;Trp ⁴²⁻¹⁰	Laboratory of Dr. Jos Jonkers	N/A
Mouse: KB1P: FVB/N-K14cre;Brca1 ^{Δ5-13} ;Trp ⁴²⁻¹⁰	Laboratory of Dr. Jos Jonkers	N/A
Mouse: KB2P: 129/Ola,FVB/N-K14cre;Brca2 ^{Δ11} ;Trp ⁴²⁻¹⁰	Laboratory of Dr. Jos Jonkers	N/A
Mouse: KB1B2P: 129/Ola,FVB/N-K14cre;Brca1 ^{Δ5-13} ,Brca2 ^{Δ11} ,Trp ⁴²⁻¹⁰	Laboratory of Dr. Jos Jonkers	N/A
Mouse: WP: 129/Ola,FVB/N-WAPcre;Trp ⁴²⁻¹⁰	Laboratory of Dr. Jos Jonkers	N/A
Mouse: WB1P: 129/Ola,FVB/N-WAPcre;Brca1 ^{Δ5-13} ,Trp ⁴²⁻¹⁰	Laboratory of Dr. Jos Jonkers	N/A
Software and Algorithms		
SpeedSeq	Chiang et al., 2015	N/A
NBIC-seq	Xi et al., 2011	N/A
Crest	Wang et al., 2011	N/A
Delly	Rausch et al., 2012	N/A
BreakDancer	Chen et al., 2009	N/A
Hydra-Multi	Lindberg et al., 2015	N/A
mclust R package	https://cran.r-project.org/web/packages/mclust/mclust.pdf	N/A
lmerTest R package	Kuznetsova et al., 2017	https://cran.openCPU.org/web/packages/lmerTest/lmerTest.pdf
pastecs R package	https://cran.r-project.org/web/packages/pastecs/pastecs.pdf	N/A
Critical Commercial Assays		
KAPA Hyper Prep Kit	KAPA Biosystems	Cat#KK8505

CONTACT FOR REAGENT AND RESOURCE SHARING

Further information and requests for resources and software should be directed to and will be fulfilled by the Lead Contact, Edison T. Liu (ed.liu@jax.org).

EXPERIMENTAL MODEL AND SUBJECT DETAILS

PDXs

TNBC PDX models were established at The Jackson Laboratory campus, as previously described (Menghi et al., 2016). All animal procedures were approved by The Jackson Laboratory Institutional Animal Care and Use Committee (IACUC) under protocol number 12027.

Mouse Models of Breast Cancer

Mouse models of breast cancer were established in the Jos Jonkers lab, as previously described (Jonkers et al., 2001; Liu et al., 2007), in compliance with local and international regulations and ethical guidelines, and under authorization by the local animal experimental committee at the Netherlands Cancer Institute (DEC-NKI).

METHOD DETAILS

Data Collection for TDP Classification

A catalogue of somatic tandem duplications (TDs) in human cancer was compiled from a number of published studies and a variety of sources, including The Cancer Genome Atlas (TCGA), the International Cancer Genome Consortium (ICGC) and the Catalogue Of Somatic Mutations In Cancer (COSMIC). In cases where data from two or more tumor samples from the same patient donor was available, only one sample was selected for analysis. Priority was granted to primary tumors and tumors with the highest sequence coverage. In addition, 16 patient-derived xenograft (PDX) models of Triple Negative Breast Cancer (TNBC) were sequenced in-house. In total, 2717 tumor genomes from as many independent donors were assessed for the presence, genomic distribution and span size of somatic tandem duplications. The vast majority of the analyzed samples were primary solid tumors ($n = 2,451$). The dataset also included 75 metastatic solid tumors, 8 solid tumor recurrences, 18 PDXs, 55 cell lines, 98 blood tumors and 12 ascites samples (Table S3).

TCGA Cohort Data Collection and Processing

Whole Genome Sequencing (WGS) data for the 992 TCGA tumors analyzed in this study has been collected from the Cancer Genomics Hub (<https://cghub.ucsc.edu/>). Raw reads were aligned against the reference genome *Hg19* and SpeedSeq (Chiang et al., 2015) was used to identify somatic rearrangements, as previously described (Barthel et al., 2017). Only tandem duplications with quality scores of 100 or greater and with both paired-end and split-read support were selected for TDP analysis, as these criteria have been reported to provide the highest confidence call set (Chiang et al., 2015). A list of all TCGA tumor samples analyzed with their corresponding number of somatic tandem duplications is part of Table S3.

Other Publicly Available WGS Cancer Cohorts

WGS-based somatic structural variation calls from three studies (Connor et al., 2017; Ferrari et al., 2016; Fujimoto et al., 2016) were downloaded from the ICGC Data Portal (<https://dcc.icgc.org/>) in November 2016 (data freeze version 22). WGS-based somatic structural variation calls from 13 other studies (Bailey et al., 2016; Bass et al., 2011; Berger et al., 2011; Campbell et al., 2010; Desmedt et al., 2015; Kataoka et al., 2015; Nik-Zainal et al., 2012, 2016; Northcott et al., 2012; Patch et al., 2015; Pinto et al., 2015; Stephens et al., 2009) were downloaded from the COSMIC data portal in September 2016 (data freeze version v78). Finally, WGS-based somatic structural variation calls from 13 additional independent studies were collected from the supplementary material of their corresponding publications (Baca et al., 2013; Berger et al., 2012; Grzeda et al., 2014; Hillmer et al., 2011; Imielinski et al., 2012; Inaki et al., 2014; McBride et al., 2012; Menghi et al., 2016; Natrajan et al., 2012; Ng et al., 2012; Popova et al., 2016; Totoki et al., 2014; Yang et al., 2013). A full list of all individual tumor samples collected and analyzed is reported in Table S3, together with annotation of their original study and WGS source.

In-House WGS Cohort and Mouse Tumor Sequencing

The in-house WGS cohort consisted of 16 patient derived xenograft (PDX) TNBC models obtained from The Jackson Laboratory PDX inventory. Genomic libraries of 400 bp size were derived from the 16 PDX genomic DNA samples, using a KAPA Hyper Prep Kit according to manufacturer guidelines and 150 bp paired-end sequence reads were generated using the Illumina HiSeq X Ten system and aligned to the human genome (*Hg19*). Potential mouse contaminant reads were removed using Xenome (Conway et al., 2012). Structural variant calls were generated using four different tools (NBIC-seq (Xi et al., 2011), Crest (Wang et al., 2011), Delly (Rausch et al., 2012), and BreakDancer (Chen et al., 2009)), and high confidence events were selected when called by all four tools. In the absence of matched normal DNA samples to be used as controls, germline variants were identified as those that appear in the Database of Genomic Variants (DGV, <http://dgv.tcag.ca/>) and/or the 1,000 Genomes Project database (<http://www.internationalgenome.org>).

Mouse mammary tumors were generated in *K14-cre;Trp53^{F/F}* (KP), *WAP-cre;Trp53^{F/F}* (WP), *K14-cre;Brca1^{F/F};Trp53^{F/F}* (KB1P), *WAP-cre;Brca1^{F/F};Trp53^{F/F}* (WB1P), *K14-cre;Brca2^{F/F};Trp53^{F/F}* (KB2P) and *K14-cre;Brca1^{F/F};Brca2^{F/F};Trp53^{F/F}* (KB1B2P) female mice as described previously (Jonkers et al., 2001; Liu et al., 2007). Genomic libraries of 400 bp size were derived from 18 mouse tumor tissues and 2 mouse spleen tissues (normal controls) using a KAPA Hyper Prep Kit according to manufacturer guidelines. Mouse genomic libraries were sequenced using Illumina HiSeq 4000 to generate 150 bp paired-end sequence reads which were subsequently aligned to the mouse genome (*Mm10*). Structural variants were then predicted using a custom pipeline that combines the Hydra-Multi (Lindberg et al., 2015) and SpeedSeq (Chiang et al., 2015) algorithms. Structural variation data obtained from the two spleen DNA samples were used to remove germline variants.

The TDP Classification Algorithm

Step 1: Classification of the TCGA Cohort as the Test Set

A TDP score was computed for each tumor sample within the TCGA cohort (n=992) based on the number and chromosomal distribution of its somatic tandem duplications (TDs), as previously described (Menghi et al., 2016). Samples with no TDs but evidence of other types of somatic rearrangements and with a minimum sequence coverage of 6X were automatically scored as non-TDP.

For each one of the 118 tumors that featured a positive TDP score, we computed the span size density distribution of all the detected TDs. Using the turnpoints function of the pastecs R package, we identified the major peak of the distribution (i.e. mode) plus any additional peaks whose density measured at least 25% of the distribution mode. A total of 154 TD span size distribution peaks were identified across the 118 TDP TCGA tumors and they appeared to cluster along recurrent and clearly distinct span-size intervals (Figure S1). To resolve the underlying distribution of the 154 identified TD span size distribution peaks, we used the Mclust function of the mclust R package and fit different numbers of mixture components (up to nine) to the peak distribution, using default estimates as the starting values for the iterative procedure. We compared the resulting mixture model estimates using the Bayesian information criterion and found that a mixture model comprising five Gaussian distributions with equal variance corresponded to the optimal fit. We then identified five non-overlapping span size intervals by setting thresholds corresponding to the intersections between each pair of adjacent Gaussian curves (<1.64 Kb, 1.64–51 Kb, 51–622 Kb, 622 Kb–6.2 Mb, >6.2 Mb) (Figure S1). Based on these thresholds, we were able to classify each TD span size distribution peak as well as each individual TD into one of 5 span size classes (classes 0-4, Figure S1).

Finally, we sub-grouped TDP tumors based on the presence of specific peaks/peak combinations, which appeared to be highly prevalent across the 118 TCGA TDP tumors. Tumors featuring a TD span size modal distribution were designated as TDP group 1, TDP group 2 and TDP group 3 based on the presence of a single TD span size distribution peak classified as class 1, class 2 and class 3, respectively. Similarly, tumors featuring a TD span size bimodal distribution were designated as TDP group 1/2mix (featuring class 1 and class 2 peaks), TDP group 1/3mix (featuring class 1 and class 3 peaks) and TDP group 2/3mix (featuring class 2 and class 3 peaks) (Figure 1A and Table S2). Only one out of the 118 TDP tumors did not fit any of these profiles as it featured a class 0 peak and a class 4 peak but none of the class 1, class 2 or class 3 peaks. We labeled this tumor as unclassified and did not include it in any further analysis.

Step 2: Validation of the TDP Classification Algorithm on an Independent Collection of Sample Cohorts

The TDP classification algorithm developed using the TCGA cohort as test set was applied to a completely independent dataset of 1725 tumor samples from individual patient donors, assembled from 30 different studies (referenced above) and representing 14 different tumor types. The algorithm performed consistently and robustly across the different studies of the validation cohort, by classifying 99% of the 258 TDP tumors in this cohort (257/258) into one of the six TDP subgroup profiles identified using the TCGA cohort, and by replicating similar frequencies of TDP subgroup occurrences within specific tumor types.

SNV Association Analysis

Somatic single nucleotide variation (SNV) data for the tumor samples analyzed in this study was downloaded in September 2016 from the COSMIC data portal (data freeze version v78). Only tumor samples classified as breast, ovarian or endometrial carcinomas and for which whole genome or whole exome sequencing data were available were considered for the SNV-TDP group association analysis (n = 678, see Table S3). Only potentially damaging somatic variants were included in this analysis and comprised nonsense, frame-shift, splice site and missense mutations. Candidate genes associated with specific TDP states were considered those whose mutation rate was at least 10% and was specifically associated with only one distinct TDP profile and not any other, nor with non-TDP tumors. The significance of the associations was determined via Fisher's exact test. Given the large number of genes tested (n=17,332) and the relatively modest number of available samples for each TDP subgroup, none of the associations reached statistical significance after correcting for multiple testing. Nonetheless, non-corrected p values were utilized to rank genes and to identify the most likely candidates. Only two candidate genes emerged from this analysis (*CDK12* in TDP group 2/3mix and *FBXW7* in TDP group 2), and their association with the specific TDP subgroups was cross-validated by existing literature reports (*CDK12* TD plus phenotype described by Popova et al. (Popova et al., 2016), in the case of *CDK12*) or alternative yet complementing gene mutations (*CCNE1* amplification in the case of *FBXW7*).

CNV Association Analysis

The discovery phase of the copy number variant (CNV) association analysis was performed on the TCGA pan-cancer dataset, to allow for homogenously processed copy number information. Gene-based copy number calls relative to 977 tumor samples were

obtained from the UCSC Cancer Genomic Browser (<https://genome-cancer.ucsc.edu>) (dataset ID: TCGA_PANCAN_gistic2, version: 2015-02-06) (Table S3). A liner mixed model (LMM) was used to identify the effect of TDP groups on copy number variations while controlling the variation from multiple tissues by including the tumor issue variable as random effect. Statistical analysis was performed using the package lmerTest (Kuznetsova et al., 2017) in R (version 3.3.0). P values were adjusted for multiple testing using Benjamini-Hochberg correction. Genes were then ranked based on the p value of their association with TDP group 2 relative to TDP group 1 and, independently, to non-TDP tumors. The top genes whose copy number change was associated with TDP group 2 tumors were identified as those with the highest cumulative rank (see also Table S6).

Upon identification of the 19q12 amplicon as linked to TDP group 2 status, CNV data for the CCNE1 gene relative to the remaining tumor samples considered in this study was either retrieved from the COSMIC data portal (data freeze version v78) in the form of gene-based copy number value, or obtained from the supplementary material of the tumor samples' original publications, when available.

TD Breakpoint Analysis

Somatic TDs occurring across the entire pan-cancer dataset analyzed in this study (2717 tumor samples) were categorized into 4 classes as follows (also see Figure S4A):

- (a) Class 1 TDs (~11 Kb) occurring in TDP tumors featuring a class 1 TD span size distribution peak (i.e. TDP groups 1, 1/2mix and 1/3mix; n = 22,447 TDs);
- (b) Class 2 TDs (~231 Kb) from TDP tumors with a class 2 TD span size distribution peak (i.e., TDP groups 2, 1/2mix and 2/3mix; n = 9794 TDs);
- (c) Class 3 TDs (~1.7 Mb) from TDP tumors with a class 3 TD span size distribution peak (i.e. TDP groups 3, 1/3mix and 2/3mix; n = 2,586 TDs) and
- (d) Non-TDP TDs, i.e. all TDs occurring in non-TDP tumors, regardless of their individual span size (n = 25,397 TDs).

TD coordinates originally annotated using older genome assemblies were converted to the GRCh38/hg38 human genome version using the LiftOver tool of the UCSC Genome Browser (<https://genome.ucsc.edu/index.html>).

All of the breakpoint coordinates relative to each TD class were then binned into consecutive, non-overlapping 500 Kb genomic windows. A TD breakpoint background distribution was generated by shuffling the TD coordinates 1,000 times. At each iteration, the genomic locations of the TDs were randomly permuted across the entire genome with the exclusion of centromeric and telomeric regions, while preserving TD numbers and span sizes. Genomic hotspots for TD breakpoints were identified as 500 Kb genomic windows with an observed number of breakpoints larger than the average count value obtained from the background distribution, plus 5 standard deviations.

Analysis of Recurrently TD-Impacted Genes

TD-impacted genes were identified as those genes whose genomic location overlapped with that of one or more TDs. Every instance in which a gene and a TD featured some degree of genomic overlap was flagged as either (i) duplication (DUP), when the TD spanned the entire length of the gene body resulting in gene duplication; (ii) double transection (DT), when both TD breakpoints fell within the gene body resulting in the disruption of gene integrity or (iii) single transection (ST), when only one TD breakpoint fell within a target gene body, resulting in a *de facto* gene copy number neutral rearrangement. For each TD class (Figure S4A) and each tumor type examined, we computed the frequency with which any given gene appeared to be impacted in one of the three possible ways (i.e. DUP, DT or ST) and assigned empirical p values to these occurrences based on the number of times, out of 1,000 iterations, that a random permutation of the TD genomic locations would result in a similar or higher frequency. Recurrently TD-impacted genes were identified as those that appeared to be affected by TDs in any one of the three possible ways in at least 5% of the tumor samples examined and in a minimum of 3 tumor samples, and with a p value < 0.05. The full list of recurrently TD-impacted genes is provided in Table S8.

Cancer Gene Lists

Breast Cancer Survival Genes

Genes associated with breast cancer patients' prognosis data (good and poor prognosis genes) were identified as previously described (Inaki et al., 2014).

Known Cancer Genes

Lists of known tumor suppressor genes (TSGs) and oncogenes (OGs) were generated described before (Menghi et al., 2016).

Davoli Cancer Genes

Tumor suppressor genes (TSGs) and oncogenes (OGs) identified by Davoli et al. (Davoli et al., 2013).

Analysis of Disease-Associated Single Nucleotide Polymorphisms (SNPs) and Tissue-Specific Super-Enhancers

Lists of tissue-specific super-enhancers and disease-associated SNPs relative to breast and ovarian tissues were obtained from Hnisz et al. (Hnisz et al., 2013). For both tumor types examined (TNBC and OV), and for each one of the 3 major classes of TDs occurring in TDP tumors (Figure S4A), we computed the percentage of TDs that results in the duplication of SNPs and, separately,

super-enhancers. The chi-squared test was used to compare the observed percentage to the expected one, computed as the mean value obtained from 1,000 random permutations of the TD genomic locations, as described above.

Analysis of Topologically Associating Domains (TADs)

Genomic coordinates relative to the full catalogue of TADs for the B lymphoblastoid cell line GM12878 were published before (Tang et al., 2015). For both tumor types examined (TNBC and OV), and for each one of the 3 major classes of TDs occurring in TDP tumors (Figure S4A), we computed the percentage of TDs that overlap with TAD boundaries by at least one base pair. To compute the expected TD genomic distribution, genomic fragments were randomly sampled from non-centromere and non-telomere genomic region, with the requirement that the lengths of the sampled fragment fit the length distribution of the observed TDs. The randomly sampled fragments were then mapped to the TAD boundaries to calculate the expected percentage of TDs that overlap with TAD boundaries. The mean and standard deviation of the number of random fragments that overlap TAD boundaries were computed from 1,000 random permutations. The chi-squared test was used to compare the observed and expected values.

DATA AND SOFTWARE AVAILABILITY

WGS data relative to both the in-house sequenced cohort (i.e. 16 PDX TNBC models) and the mouse breast cancer models are available from the Sequence Read Archive database (www.ncbi.nlm.nih.gov/sra), SRA: PRJNA430898.

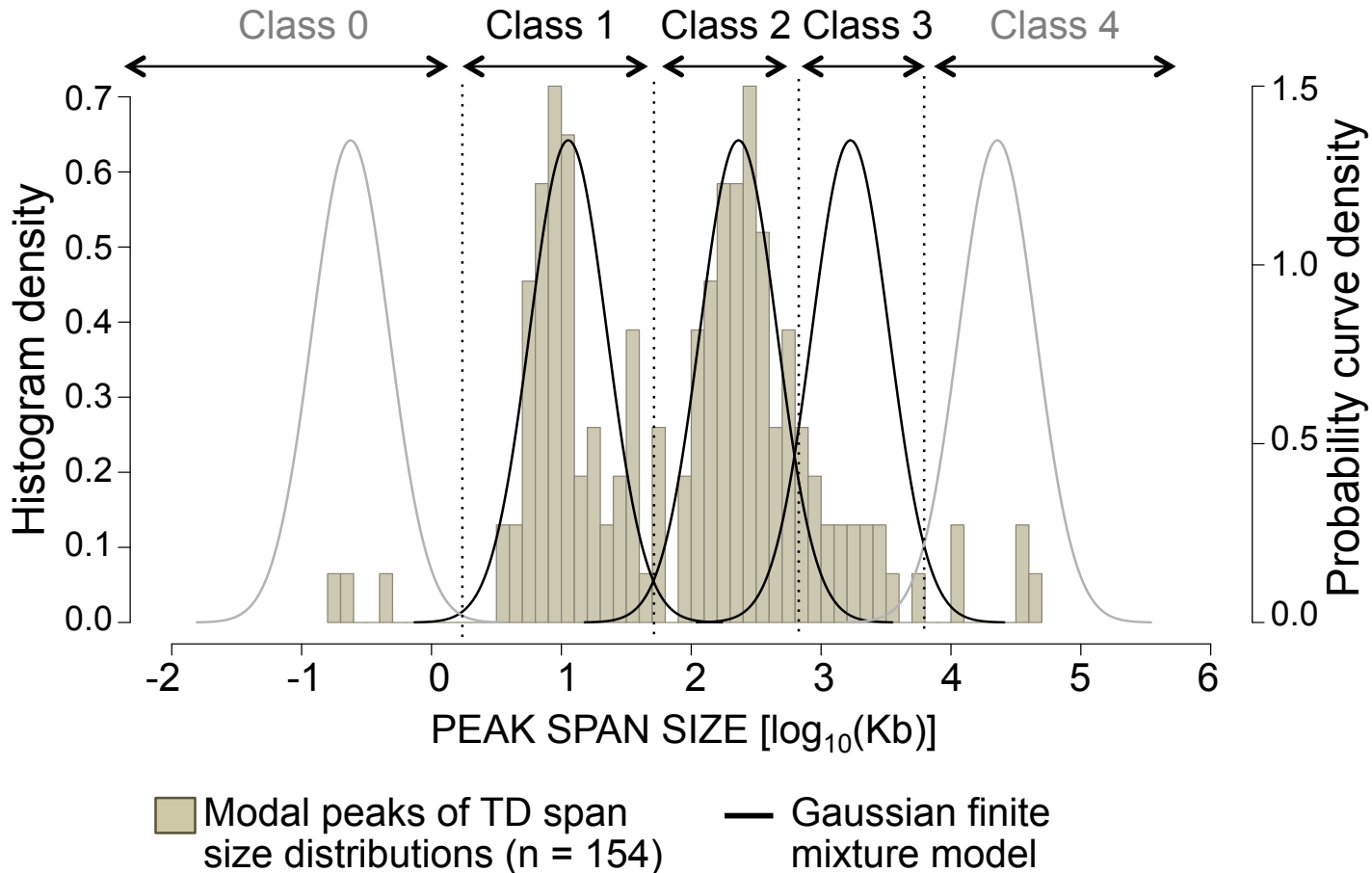
QUANTIFICATION AND STATISTICAL ANALYSIS

Unless otherwise stated, statistical analysis was performed and graphics produced using the R statistical programming language version 3.3.2 (www.cran.r-project.org). All hypothesis tests were two-sided when appropriate and the precise statistical tests employed are specified in Results and corresponding figure legends.

Supplemental Information

The Tandem Duplicator Phenotype Is a Prevalent Genome-Wide Cancer Configuration Driven by Distinct Gene Mutations

Francesca Menghi, Floris P. Barthel, Vinod Yadav, Ming Tang, Bo Ji, Zhonghui Tang, Gregory W. Carter, Yijun Ruan, Ralph Scully, Roel G.W. Verhaak, Jos Jonkers, and Edison T. Liu



■ Modal peaks of TD span size distributions ($n = 154$) — Gaussian finite mixture model

TD/TD peak class	Span size range	Distribution median	Distribution standard deviation	No. modal peaks (tot = 154)
class 0	<1.64 Kb	0.2 Kb	1.98 Kb	3
class 1	1.64 Kb-51 Kb	11.3 Kb	1.98 Kb	60
class 2	51 Kb-622 Kb	231.2 Kb	1.98 Kb	67
class 3	622 Kb-6.2 Mb	1.7 Mb	1.98 Kb	19
class 4	>6.2 Mb	22.8 Mb	1.98 Kb	5

Figure S1, related to Figure 1. Classification of TD span size distribution peaks.

Histogram: density profile of 154 TD span size distribution peaks, relative to the 118 TDP genomes included in the TCGA training pan-cancer dataset. Curves: five normal distributions sharing equal variants are identified as the best Gaussian finite mixture model to fit the TD span size peak distribution, according to the EM algorithm. Thresholds for the identification of the five TD span size intervals (i.e. classes 0-4) were set at the intersection between each pair of adjacent curves (dotted lines). Median and standard deviation values for each curve are reported in the table, together with upper and lower limits of the five identified span size intervals.

Classes 1-3 comprise 146 of the 154 (94.8%) TD span size distribution peaks identified and were used to classify TDP tumors into one of six distinct TDP subgroups, as illustrated in Figure 1B.

Table S2, related to Figure 1. TD span size distribution modal peaks across the TCGA dataset (992 tumors, 118 TDPs)

class 0 [<1.64 Kb]	class 1 [1.64 Kb-51 Kb]	class 2 [51 Kb-622 Kb]	class 3 [622 Kb-6.2 Mb]	class 4 [>6.2 Mb]	Frequency	%	cumulative %	TDP_classification
		✓			41	34.7	34.7	TDP group 2
✓					38	32.2	66.9	TDP group 1
✓	✓				13	11.0	78.0	TDP group 1/2mix
	✓	✓			8	6.8	84.7	TDP group 2/3mix
✓		✓			6	5.1	89.8	TDP group 1/3mix
		✓			5	4.2	94.1	TDP group 3
	✓		✓		2	1.7	95.8	TDP group 2
✓			✓		2	1.7	97.5	TDP group 1
✓	✓				2	1.7	99.2	TDP group 2
✓			✓		1	0.8	100.0	Unclassified

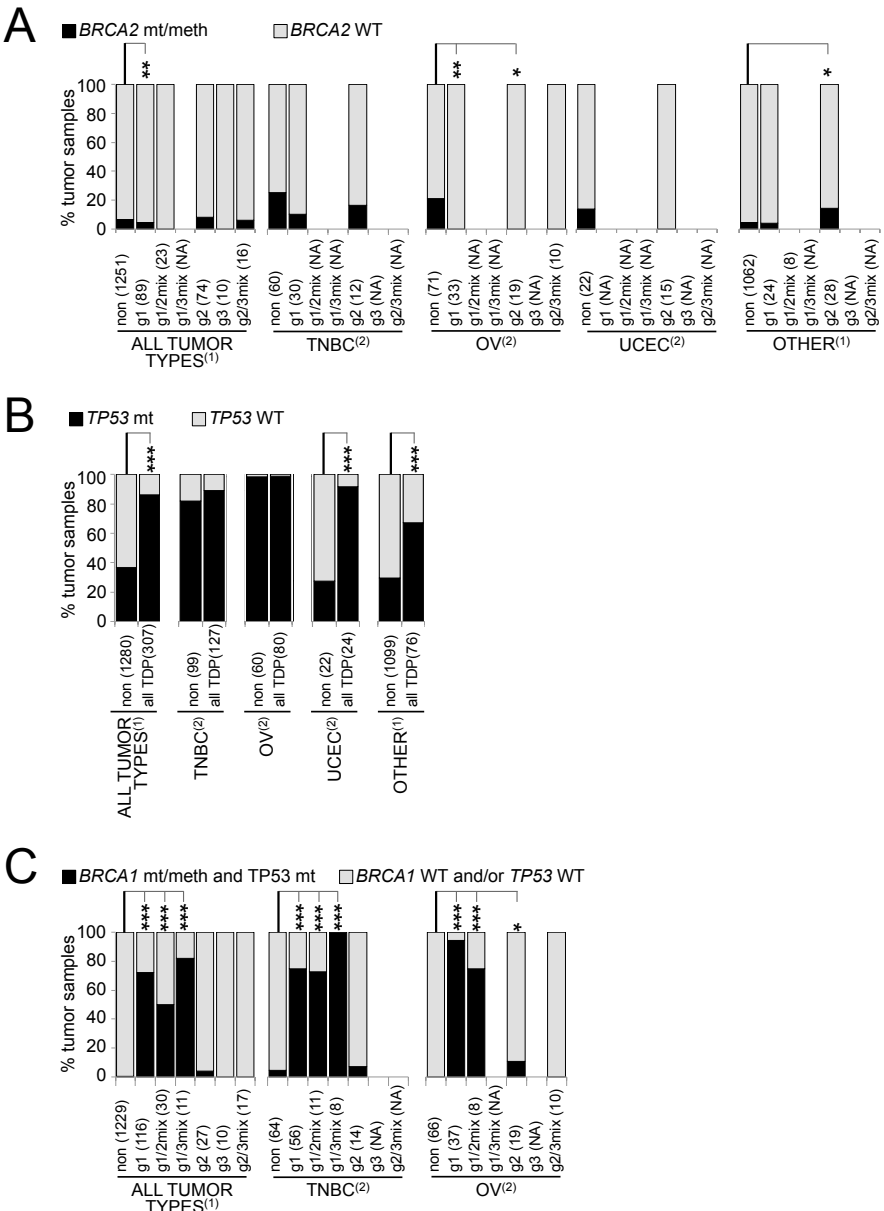


Figure S2, related to Figure 2. Combined abrogation of *BRCA1* and *TP53*, but not of *BRCA2* is specifically found in the large majority of TDP tumors featuring class 1 TDs.

(A) Percentage of tumor samples featuring abrogation of the *BRCA2* gene via germline or somatic mutation, promoter methylation or gene rearrangement.

(B) Percentage of tumor samples featuring abrogation of the *TP53* gene by somatic mutation.

(C) Percentage of tumor samples featuring combined abrogation of both the *BRCA1* and *TP53* genes.

Only tumor type/TDP group combinations comprising at least eight tumor samples are analyzed. NA: data not available; non: non-TDP tumors; g1, g1/2mix, g1/3mix, g2, g3, g2/3mix: TDP groups 1, 1/2mix, 1/3mix, 2, 3 and 2/3mix ; OTHER: all tumor types except TNBC, OV and UCEC. ***p<0.001, **p<0.01, *p<0.05, by ⁽¹⁾generalized linear mixed model with tumor type as the random effect or ⁽²⁾Fisher's exact test.

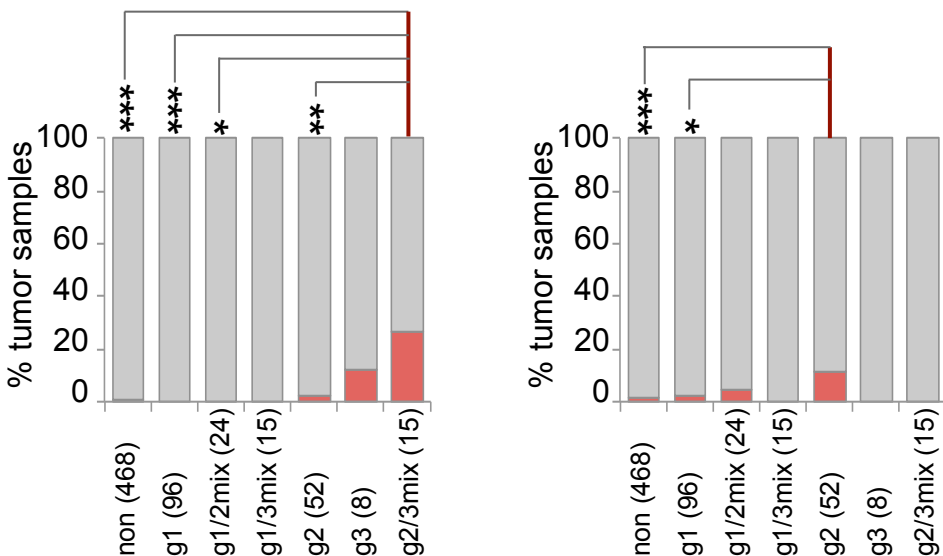
Table S5, related to Figure 2. Summary Table of whole genome sequencing results for 18 mouse breast tumors.

Tumor	GEM model	Cre transgene	Genotype	TDP status	TDPscore	No_TD	PEAK CLASS
#1	<i>Trp53^{F/F}</i>	<i>K14cre</i>	<i>Trp53^{A/A}</i>	NON TDP	-0.37	10	none
#2	<i>Trp53^{F/F}</i>	<i>K14cre</i>	<i>Trp53^{A/A}</i>	NON TDP	-1.07	2	none
#3	<i>Trp53^{F/F}</i>	<i>K14cre</i>	<i>Trp53^{A/A}</i>	NON TDP	-0.92	44	class 0, class 4
#4	<i>Trp53^{F/F}</i>	<i>WAPcre</i>	<i>Trp53^{A/A}</i>	NON TDP	-1.07	7	none
#5	<i>Trp53^{F/F}</i>	<i>WAPcre</i>	<i>Trp53^{A/A}</i>	NON TDP	-0.91	6	none
#6	<i>Trp53^{F/F}</i>	<i>WAPcre</i>	<i>Trp53^{A/A}</i>	NON TDP	-2.00	0	none
#7	<i>Trp53^{F/F}; Brca1^{F/F}</i>	<i>K14cre</i>	<i>Trp53^{A/A}; Brca1^{A/A}</i>	TDP group 1	0.15	39	class 1
#8	<i>Trp53^{F/F}; Brca1^{F/F}</i>	<i>K14cre</i>	<i>Trp53^{A/A}; Brca1^{A/A}</i>	NON TDP*	-0.23	56	class 1, class 4
#9	<i>Trp53^{F/F}; Brca1^{F/F}</i>	<i>K14cre</i>	<i>Trp53^{A/A}; Brca1^{A/A}</i>	TDP group 1	0.02	61	class 1, class 4
#10	<i>Trp53^{F/F}; Brca1^{F/F}</i>	<i>WAPcre</i>	<i>Trp53^{A/A}; Brca1^{A/A}</i>	TDP group 1	0.18	58	class 1
#11	<i>Trp53^{F/F}; Brca1^{F/F}</i>	<i>WAPcre</i>	<i>Trp53^{A/A}; Brca1^{A/A}</i>	TDP group 1	0.03	78	class 1, class 4
#12	<i>Trp53^{F/F}; Brca1^{F/F}</i>	<i>WAPcre</i>	<i>Trp53^{A/A}; Brca1^{A/A}</i>	TDP group 1	0.04	44	class 1, class 4
#13	<i>Trp53^{F/F}; Brca2^{F/F}</i>	<i>K14cre</i>	<i>Trp53^{A/A}; Brca2^{A/A}</i>	NON TDP	-0.81	8	none
#14	<i>Trp53^{F/F}; Brca2^{F/F}</i>	<i>K14cre</i>	<i>Trp53^{A/A}; Brca2^{A/A}</i>	NON TDP	-0.59	25	class 4
#15	<i>Trp53^{F/F}; Brca2^{F/F}</i>	<i>K14cre</i>	<i>Trp53^{A/A}; Brca2^{A/A}</i>	NON TDP	-0.77	13	none
#16	<i>Trp53^{F/F}; Brca1^{F/F}; Brca2^{F/F}</i>	<i>K14cre</i>	<i>Trp53^{A/A}; Brca1^{A/A}; Brca2^{A/A}</i>	TDP group 1	0.13	68	class 1, class 4
#17	<i>Trp53^{F/F}; Brca1^{F/F}; Brca2^{F/F}</i>	<i>K14cre</i>	<i>Trp53^{A/A}; Brca1^{F/F}; Brca2^{A/A}</i>	NON TDP	-0.46	34	class 3
#18	<i>Trp53^{F/F}; Brca1^{F/F}; Brca2^{F/F}</i>	<i>K14cre</i>	<i>Trp53^{A/A}; Brca1^{A/F}; Brca2^{A/A}</i>	NON TDP	-0.66	16	none

Tumors with a class 1 TD span size distribution peak are highlighted in red.

* This tumor sample classifies as NON TDP but features the TD class 1 peak characteristic of TDP group 1 genomes.

A ■ *CDK12* mt □ *CDK12* WT **B** ■ *FBXW7* mt □ *FBXW7* WT



C

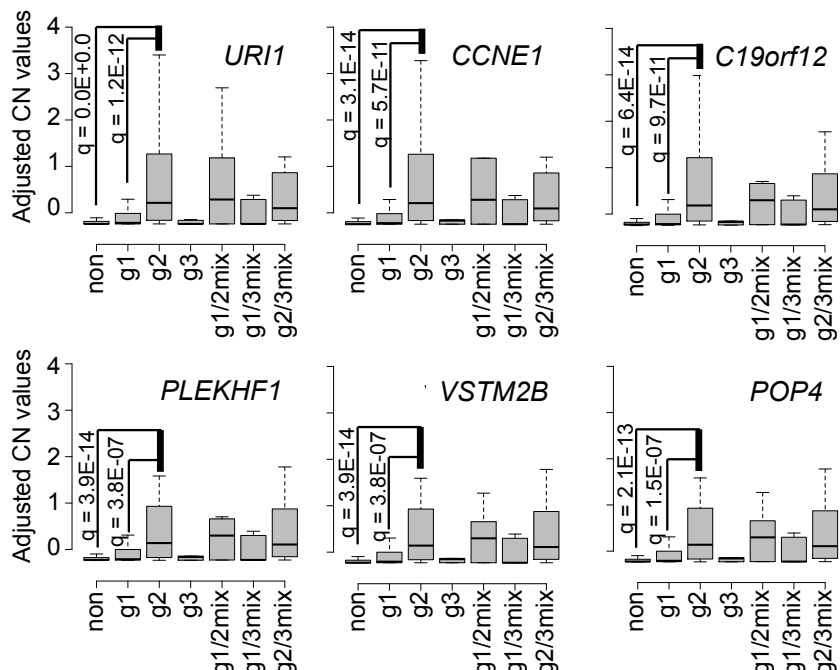


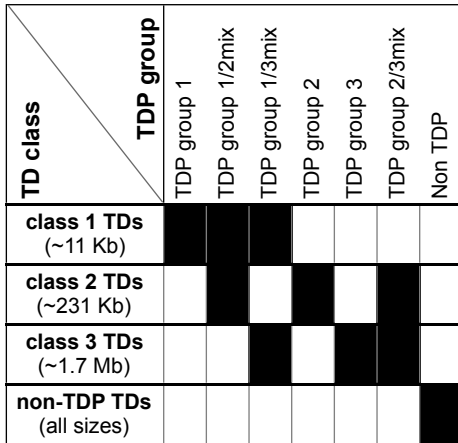
Figure S3, related to Figure 3. Genetic perturbations in non-BRCA1-linked TDP groups.

(A, B) SNV exploratory analysis: *FBXW7* and *CDK12* mutation rates across TDP subgroups. The analysis was performed on the combined breast, ovarian and endometrial carcinoma datasets comprising a total of 678 tumors for which both somatic SNV and WGS data are available. (A) *CDK12* mutation rate. Fisher's exact test: mix23 vs. non: OR=40.6, P=4.0E-05; g2/3mix vs. g1: OR=inf, P=2.3E-04; g2/3mix vs. g2: OR = 17.4, p = 7.7E-03; g2/3mix vs. g1/2mix: OR = inf, p = 1.7E-02. (B) *FBXW7* gene mutation rate. Fisher's exact test: g2 vs. non: odds ratio [OR] = 10, p = 4.4E-04; g2 vs. g1: OR = 6.1, p = 2.3E-02.

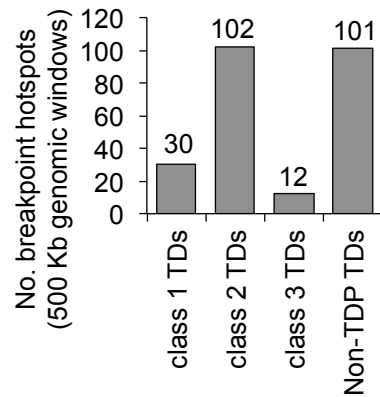
(C) Chr 19q12 gene amplification in TDP group 2 tumors. Boxplots depict the copy number distribution profile across TDP subgroups for the top six candidate genes associated with TDP group 2 in a LMM copy number analysis of the TCGA pan-cancer dataset (n = 977 tumors). All six genes map to the 19q12 amplicon and show a significant copy number increase in TDP group 2 tumors compared to non-TDP and TDP group 1 tumors (q: q-values, i.e. Benjamini-Hochberg corrected p-values). The distribution of adjusted CN values for TDP groups 3, 1/2mix, 1/3mix and 2/3mix are also shown for comparison. Boxes span the interquartile range, with the median values marked by a horizontal line inside the box. Whiskers extend to 1.5 times the interquartile range from each box.

Abbreviations: non: non-TDP tumors; g1, g1/2mix, g1/3mix, g2, g3, g2/3mix: TDP groups 1, 1/2mix, 1/3mix, 2, 3 and 2/3mix.

A



B



C

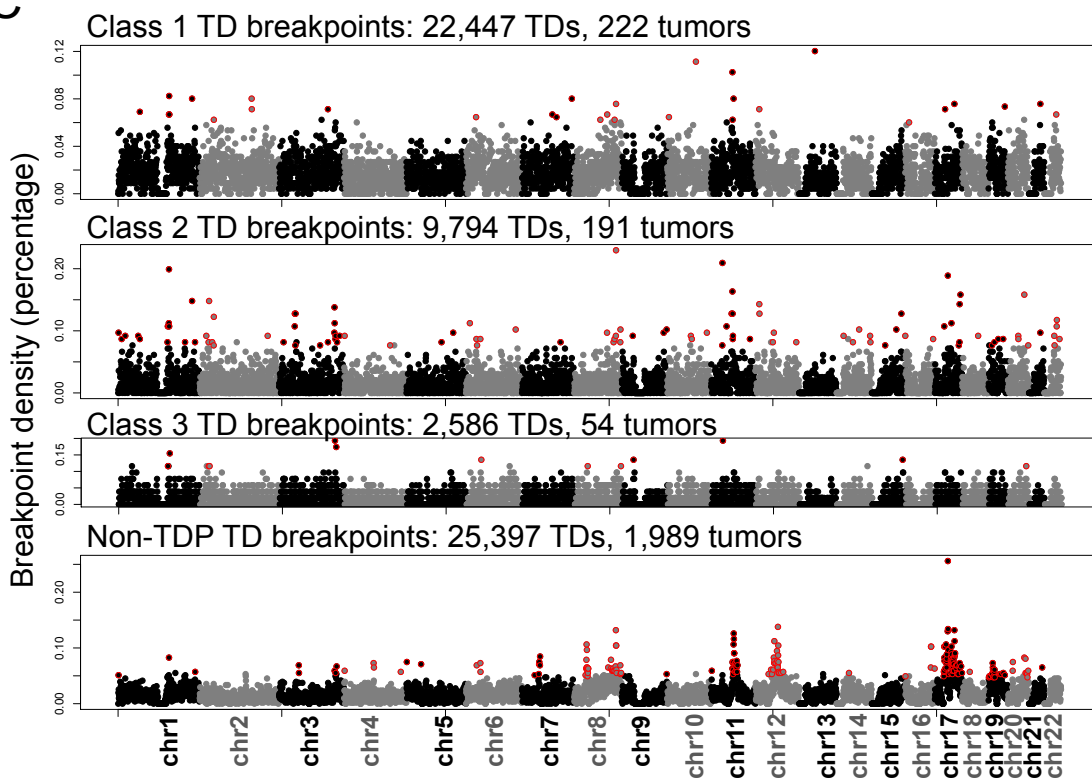
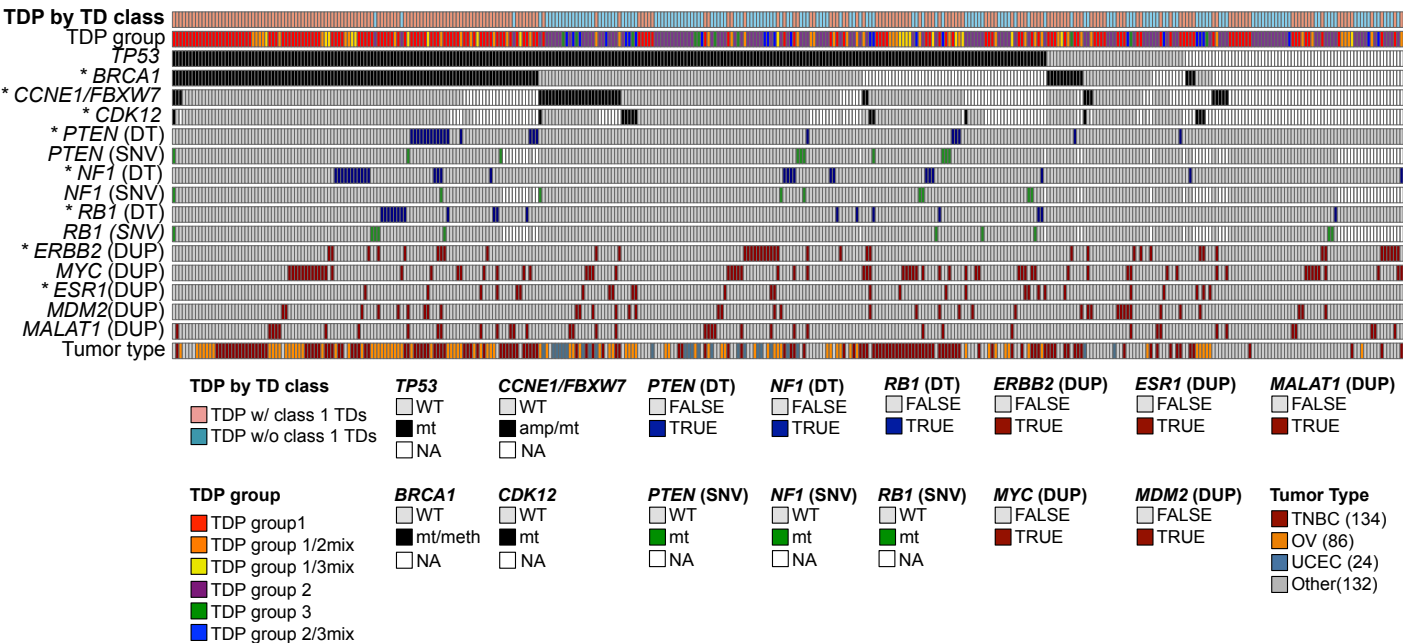


Figure S4, related to Figure 4. Analysis of TD breakpoint hotspots.

- (A) Schematic overview of the four classes of TDs considered for the breakpoint analysis.
- (B) Number of significant breakpoint hotspots identified across the four classes of TDs examined. Breakpoint hotspots are defined as 500 Kb genomic windows with a number of breakpoints higher than the average value obtain from 1,000 random permutation of the TD coordinates, plus 5 standard deviations.
- (C) TD breakpoint density per 500 Kb windows along the entire genome. Breakpoint hotspots are indicated in red and coincide with those represented in **Figure 4**. Class 2 TDs and non-TDP TDs are involved in a comparable number of breakpoint hotspots ($n = 102$ and 101 for class 2 and non-TDP TDs, respectively), however, their genomic distributions is remarkably different, with non-TDP TD hotspots clustering around few chromosomal locations and class 2 TD hotspots being more homogenously distributed along the entire genome.

A



B

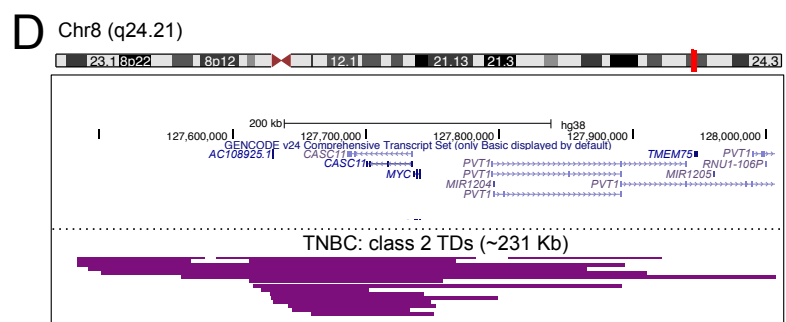
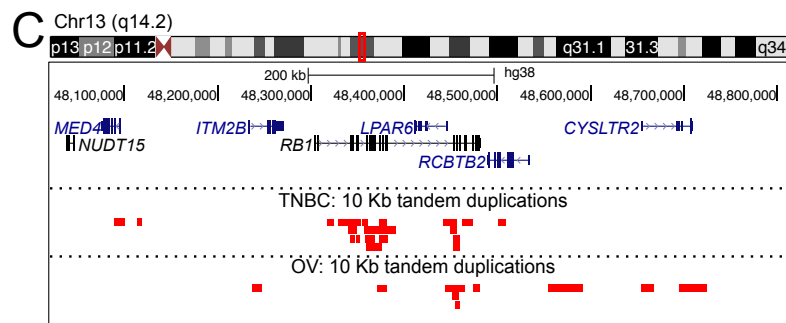
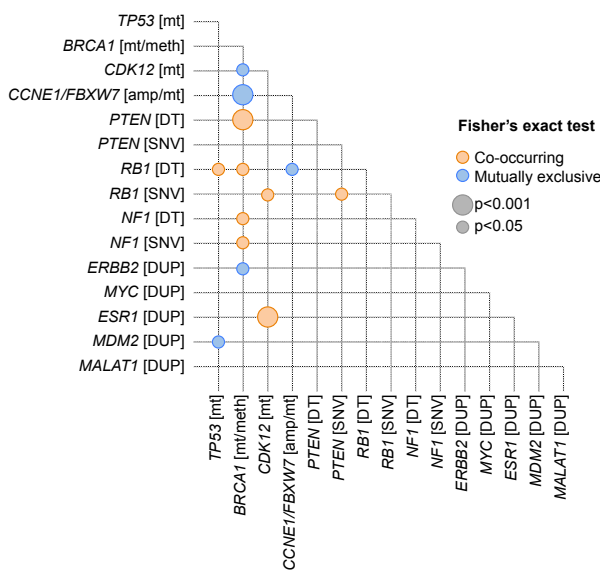


Figure S5, related to Figure 5. Top cancer genes most recurrently affected by TDs in TDP tumors.

(A) Summary view of the major genetic perturbations and genomic consequences associated with the different TDP subgroups. Only TDP tumors (n=376) are depicted in this graph. DT, double transection via TD; DUP, duplication via TD. *: variables significantly associated with TDP subgrouping (TDP by TD class) by means of Fisher's exact test.

(B) Pairwise associations among TDP putative drivers and top TD-impacted genes, as depicted in (A). Only significant associations are shown ($p<0.05$). Orange and blue circles indicate co-occurring and mutually exclusive pairs, respectively. Among TDP putative drivers, loss of *BRCA1* is mutually exclusive with activation of the *CCNE1* pathway (via *CCNE1* gene amplification or *FBXW7* gene mutation) and *CDK12* gene mutation. On the other hand, loss of *BRCA1* is significantly associated with disruption of the *PTEN*, *RB1* and *NF1* tumor suppressor genes via TD-mediated double transection in tumor samples that would otherwise be wild-type for these genes.

(C) High density of class 1 TDs at the *RB1* locus in both the TNBC and OV datasets.

(D) High density of class 2 TDs at the *MYC* locus in the TNBC dataset.

Table S9, relative to Figure 6. SNP/super-enhancer and TAD boundary duplication via TDs.

Tumor type	TD class	SNP/super-enhancer			TAD boundary		
		No. and % of TDs engaged in SNP/super-enhancer duplication (OBSERVED)	No. and % of TDs engaged in SNP/super-enhancer duplication (EXPECTED, mean)	Chi-squared test	No. and % of TDs engaged in TAD boundary duplication (OBSERVED)	No. and % of TDs engaged in TAD boundary duplication (EXPECTED, mean)	Chi-square test
TNBC	class 1 TDs (11 Kb)	24 (0.2%)	212 (1.5%)	2.3E-34	262 (1.9%)	235 (1.7%)	2.4E-01
TNBC	class 2 TDs (231 Kb)	404 (17.4%)	203 (8.7%)	3.2E-18	743 (32%)	610 (26.3%)	2.0E-05
TNBC	class 3 TDs (1.7 Mb)	265 (47.6%)	198 (35.5%)	6.0E-05	457 (82.3%)	429 (78.1%)	3.9E-02
OV	class 1 TDs (11 Kb)	5 (0.1%)	34 (0.8%)	7.0E-06	89 (2.2%)	76 (1.8%)	3.5E-01
OV	class 2 TDs (231 Kb)	196 (7.1%)	116 (4.2%)	4.1E-06	873 (31.6%)	740 (26.8%)	9.4E-05
OV	class 3 TDs (1.7 Mb)	344 (28.8%)	274(22.9%)	1.3E-03	1020 (86.5%)	1007 (85.4%)	4.8E-01